Geophys. J. Int. (2008) **175,** 135–152 doi: 10.1111/j.1365-246X.2008.03876.x

Structure and composition of the crust and upper mantle of the Archean–Proterozoic boundary in the Fennoscandian shield obtained by joint inversion of receiver function and surface wave phase velocity of recording of the SVEKALAPKO array

Elena Kozlovskaya,[1] Grigoriy Kosarev,[2] Igor Aleshin,[2] Oksana Riznichenko[2] and Irina Sanina[3]

[1] *Sodankylä Geophysical Observatory/Oulu Unit,* POB 3000, FIN-90014, *University of Oulu, Finland. E-mail: Elena.kozlovskaya@oulu.fi*
[2] *Institute of Physics of the Earth RAS, str. B. Gruzinskaya,* 10, *Moscow, Russia*
[3] *Institute of Geospheres Dynamics RAS, Leninsky prospect,* 38/1, *Moscow, Russia*

Accepted 2008 June 4. Received 2008 May 19; in original form 2007 September 14

SUMMARY

We present a 3-D model of absolute values of *S*-wave velocities and V_P/V_S ratios in the crust and upper mantle beneath the SVEKALAPKO temporary seismic array that covered the transition zone between Archean and Proterozoic domains in the Precambrian Fennoscandian Shield. The model was obtained using joint inversion of *P*-wave receiver functions, Rayleigh phase velocities and traveltimes of waves converted from the 410 km discontinuity. *P*-wave receiver functions and traveltimes of *Ps* waves converted from the 410 km boundary were estimated for 30 broad-band stations of the SVEKALAPKO array and short-period, small-aperture RUKSA array in Russian Karelia. The phase velocities of Rayleigh waves were taken from previous surface wave studies (Bruneton *et al.* 2004a,b). For each station, the different data sets were merged and inverted by simulated annealing method. After that, a 3-D *S*-wave velocity model and distribution of V_P/V_S ratio was obtained from 1-D velocity models, using special interpolation technique. The new 3-D seismic model demonstrates pronounced lateral variations of values of V_S and V_P/V_S ratio in the crust and uppermost mantle. The depth to the Moho boundary varies from 51 to 63 km in our model, which agrees with the results of previous controlled-source seismic studies in the region. The Moho boundary is overlain by a high-velocity lower crust (HVLC), with high V_S, which is non-uniform in composition and origin. Our study showed no systematic correlation between the lithosphere structure and tectonothermal age of Archean and Proterozoic crustal terrains in the study area. The exposed Archean–Proterozoic suture (so-called Ladoga-Bothnian Bay Zone) is not observed as a mega-scale structure in the crust and upper mantle. Generally, the Archean–Proterozoic transition occupies a larger area in the lithosphere than it was thought earlier. It is marked by a Moho depression stretching to the North and by a zone of high V_P and high V_P/V_S in the mantle. Our results supports the theory that the Fennoscandian Shield was assembled as a result of extensive collisional accretion of island arcs and microcontinental blocks and shows that these processes were working both in Archean and Proterozoic.

Key words: Inverse theory; Body waves; Surface waves and free oscillations; Cratons; Crustal structure.

1 INTRODUCTION

Structure and composition of the crust and subcrustal lithospheric mantle (SCLM) beneath Precambrian areas is still strongly debated. Recent analyses of global seismic, petrological and thermal data indicate certain dissimilarity between structure and thickness of Archean and Proterozoic lithosphere (that is, crust and underlying lithospheric mantle) and suggest that structure and composition of SCLM is related to tectonothermal age of overlying crustal terrains (Christensen & Mooney 1995; Pearson 1999; Artemieva & Mooney 2001, 2002; Griffin *et al.* 2003; Artemieva 2006). This difference, revealed by global studies, is often interpreted as a signature of fundamentally different tectonic regimes in Archean and Proterozoic. On the other hand, regional and local seismic studies in Precambrian areas show no such straightforward correlation. Generally, they demonstrate very heterogeneous and variable structure of crust and lithospheric mantle beneath both Archean and Proterozoic terrains, without visible correlation of structural features with

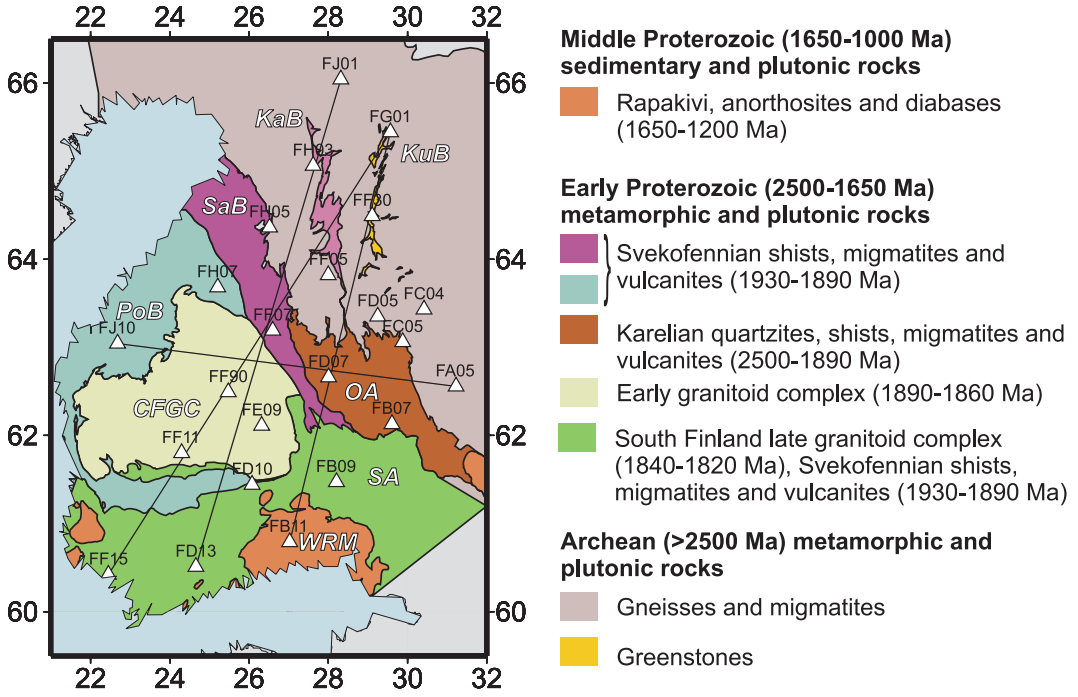

Figure 1. Simplified tectonic map of the SVEKALAPKO study area presented in WGS-84 coordinate system (adopted from Korsman *et al.* 1997; description of the legend after Korsman & Koistinen 1998). Broad-band stations used in this study are shown by white triangles. Black lines show position of cross-sections through 3-D velocity model discussed in Section 4.2. Palaeoproterozoic (*Svecofennian Domain*): (CFGC), Central Finland Granitoid Complex; SA, Saimaa area; PoB, Pohjanmaa area; SaB, Savo Belt; WRM, Wyborg Rapakivi Massif; Archaean *(Karelian Domain)*: OA, Outokumpu area; KaB, Kainuu Belt; KuB,, Kuhmo Belt.

tectonothermal age (e.g. Eaton 2006; Hjelt *et al.* 2006; Kukkonen *et al.* 2006; Darbyshire *et al.* 2007).

One of such areas is the central part of the Precambrian Fennoscandian Shield (Fig. 1), which was formed as a result of several episodes of crustal accretion starting about 3.5 Ga (Gorbatschev & Bogdanova 1993). The main tectonic divide in the central part of the Schield is a suture separating Palaeoproterozoic Svecofennian (2.1–2.3 Ga) and Archean Karelian (2.6–3.1 Ga) domains. The Karelian domain was formed during the Saamian (3.1–2.9 Ga) and Lopian (2.8–2.6 Ga) orogenies. It is composed of migmatitic trondhemite–tonalite–granodiorite (TTG) gneisses with minor greenstone rocks intruded by later granitoids. During 2.5–1.9 Ga, metasediments and metavolcanic rocks were deposited on an eroded Archean craton. The Svecofennian domain consists mainly of granitoid batholiths, surrounded by schists belts. It was formed mainly from mantle-derived juvenile material between 1.9 and 1.75 Ga, as a result of accretion of island-arcs and microcontinents to the craton (Lahtinen *et al.* 2005). The Svecofennian crust was intruded by anorogenic rapakivi batholiths, mafic dyke swarms and gabbro-anorthosites between 1.65 and 1.54 Ga in an extensional tectonic setting (Korsman *et al.* 1999).

The lithosphere structure of the central part of the Shield has been studied since 1980s and 1990s by controlled-source deep seismic sounding profiles BALTIC, SVEKA'81, SVEKA'91, FENNIA, BABEL (Luosto *et al.* 1984, 1990, 1994; Grad & Luosto 1987; BABEL Working Group 1990, 1993a,b; Sharov 1991; Yliniemi 1991; FENNIA Working Group 1998; Heikkinen & Luosto 2000). In 2001–2003 a new reflection seismic survey Finnish Reflection Experiment (FIRE), comprised four reflection seismic transects of total length of 2104 km (Kukkonen *et al.* 2006; Janik *et al.* 2007).

Controlled-source seismic studies resulted in a set of 2-D *P*-wave velocity models of the crust. The models indicated significant variations of thickness (between 42 and 65 km), structure and composition of the crust in the central part of the Fennoscandian Shield and demonstrated that the latter is essentially heterogeneous. This discovery was motivation for compilation of 3-D crustal models from results of seismic profiling. The map of the Moho topography was compiled by Luosto (1991, 1997). Later, Malaska & Hyvönen (2000) and Pavlenkova *et al.* (2001) constructed 3-D *P*-wave velocity models of the crust by interpolating and smoothing the published 2-D seismic models.

New step in understanding a 3-D structure of the lithosphere in this area was SVEKALAPKO multidisciplinary passive seismic experiment in 1998–1999 (Hjelt & Daly 1996; Bock *et al.* 2001; Hjelt *et al.* 2006). Interpretation of the SVEKALAPKO teleseismic data required improvement of a 3-D velocity model of the crust to correct teleseismic traveltimes for crustal effects in body wave tomography and constrain the structure of the crust in surface wave studies. Enhanced 3-D *P*-wave velocity models of the crust were prepared by Sandoval (2002), Sandoval *et al.* (2003) and Kozlovskaya *et al.* (2004a) from existing DSS data. However, the *S*-wave velocity model of the crust and upper mantle was not compiled because *S*-wave velocity models were obtained only for several selected profiles (Komminaho & Yliniemi 1993; Korsman *et al.* 1999; Kozlovskaya & Yliniemi 1999).

Bruneton *et al.* (2002, 2004a,b) used fundamental mode Rayleigh wave arrival times with periods between 10.5 and 190 s to investigate the *S*-wave velocity in the upper mantle, beneath the SVEKALAPKO array. As vertical resolution of this method is not sufficient to obtain detailed structure of the crust, they constrained the *S*-wave velocities in the crust. For this, they used the *P*-wave velocity model by Sandoval *et al.* (2003) and recalculated it into

S-wave velocity model using average V_P/V_S ratio for the whole crust. Bock *et al.* (2001) and Alinaghi *et al.* (2003) determined spatial variations of averaged V_P/V_S ratio in the crust using the technique by Zhu & Kanamori (2000). Due to limitations of the techniques used, these models do not show variations of either *S*-wave velocity or V_P/V_S ratio with depth.

Recently Musacchio *et al.* (1997) and Janik *et al.* (2007) demonstrated how analysis of *S*-wave velocities and V_P/V_S ratio in the crust and upper mantle can be used to infer compositional variations in the crust and to distinguish different types of crust–mantle transitions. However, their studies are limited to 2-D models only. An effort to obtain both *P*- and *S*-wave 3-D velocity models and V_P/V_S distribution in the crust down to a depth of 40 km, for the area covered by the SVEKALAPKO array, was made by Hyvönen *et al.* (2007). They used tomographic inversion of arrival times of crustal turning waves (*Pg* and *Sg*) from local events (mainly quarry blasts). As the crustal thickness in the SVEKALAPKO study region is significantly more than 40 km; the variations of V_S and V_P/V_S in the lower crust and upper mantle were not analysed.

Alternative possibility to obtain a 3-D *S*-wave velocity model of the crust and upper mantle is to use interpretation of *P*-wave receiver functions together with other data sets. This idea was recently employed by Vinnik *et al.* (2004), who used both *P*- and *S*-wave receiver functions to construct a 3-D *S*-wave velocity model of the crust and upper mantle (down to 150 km) under the Central Tien Shan. The approach was enhanced in the next study (Vinnik *et al.* 2006), where residuals of teleseismic *P*- and *S*-wave traveltimes were included in the *P* and *S* receiver function inversion. Aleshin *et al.* (2006) made joint inversion of *P* receiver function, phase velocities of Rayleigh waves and traveltimes of *Ps* waves converted from the 410 and 660 km discontinuities. Importantly, this technique allowed estimation of absolute values of *S*-wave velocity in the upper mantle, which are directly comparable to the values estimated by studies of upper-mantle xenoliths.

This paper aims to use the same approach to construct a 3-D model of absolute values of *S*-wave velocities and V_P/V_S ratios in the crust and upper mantle for the area covered by the SVEKALAPKO array. For this, we use joint inversion of *P*-wave receiver functions, Rayleigh phase velocities and traveltimes of waves converted from the 410 km discontinuity (*Ps*410). We calculate *P*-wave receiver functions for 30 broad-band SVEKALAPKO stations and small-aperture RUKSA array in Russian Karelia and measure traveltimes of *Ps*410 waves. We invert both data sets jointly with Rayleigh phase velocities determined by Bruneton *et al.* (2004a,b) and obtain a set of 1-D *S*-wave velocity models beneath selected stations of the SVEKALAPKO array. Then we calculate a 3-D *S*-wave velocity model and distribution of V_P/V_S ratio from 1-D velocity distributions using special interpolation technique.

2 DATA

2.1 Receiver function data

The SVEKALAPKO array (Fig. 1) covered the area from 59° to 68°N and 18° to 34°E. During the field campaign, 40 broad-band and 88 short-period temporary stations were installed in southern and central Finland and in western Russian Karelia, in addition to 15 existing permanent stations. The detailed description of the SVEKALAPKO seismic field experiment and data processing procedures can be found in Sandoval (2002) and Sandoval *et al.* (2003, 2004).We used waveforms of *P* waves from 23 teleseismic events (Table 1), with epicentral distances from 36° to 112° and magnitude greater than 5.9, recorded by 30 broad-band stations of the SVEKALAPKO array (Fig. 1). The SVEKALAPKO array included two small aperture subarrays: FF30, FF31, FF32, FF33 and FF90, FF91, FF92, FF93, FF94. The recordings of subarrays were stacked, and each of them was considered as a single station with

Table 1. The list of 23 events.

Date (year/month/day)	Origin time (hh:mm:ss.sss)	Latitude (°)	Longitude (°)	Depth (km)	Magnitude	Distance (°)	Backazimuth (°)	Slowness (s/°)
1998/08/20	06:40:55.820	28.932	139.329	440	7.0	76.28	55.1	5.53
1998/08/23	05:36:12.920	14.697	120.046	70	6.1	79.97	78.1	5.39
1998/08/23	13:57:15.380	11.663	−88.038	54	6.8	90.72	295.3	4.64
1998/08/30	01:48:08.760	17.092	148.133	33	6.2	90.41	52.9	4.65
1998/08/30	14:34:43.290	53.669	161.867	33	5.5	61.16	27.5	6.78
1998/09/02	08:37:29.910	5.41	126.764	50	6.8	91.26	76.8	4.62
1998/09/09	11:27:59.310	40.035	15.98	10	5.9	24.36	209.3	9.14
1998/09/14	23:16:46.830	51.618	−173.15	33	6.2	64.55	16.6	6.53
1998/09/28	13:34:30.490	−8.194	112.413	152	6.5	93.16	101.5	4.58
1998/10/03	11:15:42.690	28.505	127.615	227	6.1	67.96	70.7	6.22
1998/11/19	15:39:19.100	22.605	125.782	10	6.4	72.27	75.3	5.97
1999/01/12	02:32:25.590	26.725	140.246	440	6.1	74.81	61.2	5.65
1999/01/24	00:37:04.630	30.61	131.136	48	6.4	67.63	66.7	6.31
1999/01/28	08:10:05.420	52.86	−169.172	56	6.6	63.79	13.6	6.58
1999/03/04	05:38:26.520	28.277	57.203	37	6.6	38.22	141.4	8.41
1999/03/04	08:52:01.900	5.394	121.923	15	7.1	85.58	86.9	4.97
1999/03/05	13:01:10.950	5.249	122.119	26	5.7	85.81	86.7	4.95
1999/03/08	12:25:48.990	52.069	159.435	37	6.9	58.68	34.6	6.95
1999/03/28	19:05:11.030	30.511	79.421	23	6.6	45.68	107.2	7.91
1999/04/05	11:08:00.040	−5.632	149.625	150	7.4	110.41	62.3	4.44
1999/04/08	13:10:34.080	43.609	130.413	564	7.1	58.89	55.3	6.70
1999/05/06	23:00:53.220	29.534	51.917	33	6.3	36.22	140.1	8.53
1999/05/07	14:13:57.570	56.416	−152.939	46	6.4	62.12	359.0	6.72

Note: Distance, backazimuth and slowness are calculated for the approximate centre of SVEKALAPKO (latitude = 63°N, longitude = 27°E)

names FF30 and FF90, respectively. Thus, there were finally 23 sites or stations.

The recordings were filtered using standard Butterworth band-pass filter from 2 to 40 s. We did not use shorter periods to avoid appearance of intensive scattered waves. Unfortunately, a high level of microseismic noise in the period range 3–7 s is typical for our study region (Pedersen *et al.* 2007), and sometimes we were forced to apply additional filtering to suppress this noise. For several stations, we did not have enough data to get reliable receiver functions.

To obtain receiver functions, we used a technique similar to that described by Vinnik *et al.* (2004). Namely, the seismograms were transformed into the orthogonal ray coordinate system with L, Q and T axes. The L axis lies in the theoretical ray plane, and it is directed from the source along the motion of the P-wave. The Q axis lies in the same plane and horizontal projection of the Q axis is positive in the direction from the source. Together with the L and Q axes, the T axis forms a right-hand orthogonal triple. The L component of the signal, considered in our case as a source, is transformed into the standard form, with a deconvolution filter. The same filter is then applied to the components Q and T. After this transformation, all components were stacked. A total number of calculated receiver functions was 383.

Fig. 2 shows receiver functions from all events stacked at each of 23 broad-band stations. Two characteristic phases at delay times about 1 and 3–7s can be seen. Of them, the first one is present only in a few stations. The time and polarity of this phase indicate presence

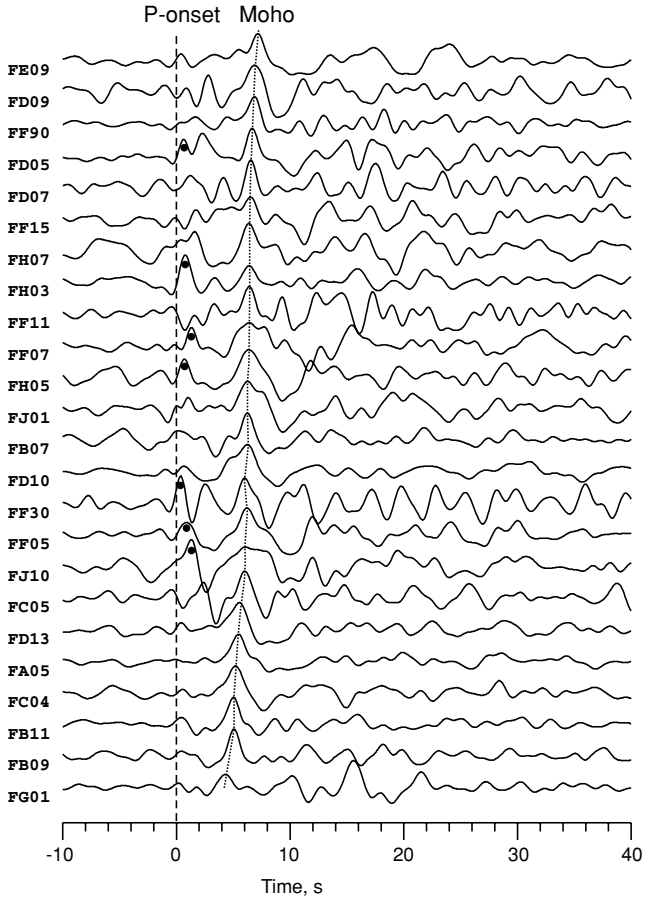

Figure 2. Summary of P receiver functions. Dashed line marks zero time. Dotted line marks *Ps* from the Moho discontinuity. Dots indicate conversion from the discontinuity in the uppermost crust.

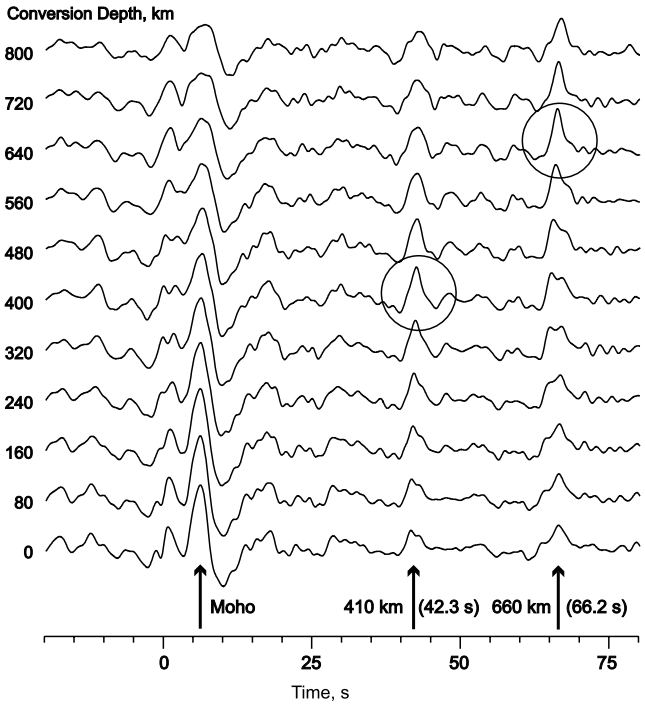

Figure 3. Stack of 383 P receiver functions. Reference distance is 67°. Delay times of *Ps* conversions from the Moho boundary and 410 and 660 km discontinuities is indicated by arrows. Circles indicate 'focusing' of correspondent conversions at certain depth. Delay times for 410 and 660 km discontinuities are 42.3 and 66.2 s, respectively.

of a thin low velocity layer and a comparatively sharp boundary in the uppermost 1–10 km of the crust. The second one is conversion from the Moho boundary, clearly seen in all records.

Stacks of P receiver functions over all stations and events are shown in Fig. 3, where clear conversions from the 410 and 660 km boundaries (*Ps*410 and *Ps*660) can be seen. As it was shown in Ammon *et al.* (1990) and Julia *et al.* (2000), additional data are necessary to stabilize solution to the inversion for the velocity structure based on receiver function data. In this study, traveltime of *Ps*410 and Rayleigh phase velocities were used as additional optimization constraints.

2.2 Traveltime of the wave converted from the 410-km boundary

Introduction into the inversion of traveltime of the P-wave converted from the upper boundary of mantle transition zone at a depth of 410 km (*Ps*410) has not been previously used in conventional receiver function studies. The first successful attempt was made by the authors while reconstructing the crustal structure under RUKSA seismic array using short-period seismic data (Aleshin *et al.* 2006).

Following the technique originally proposed by Vinnik (1977), we calculated a stack with move-out time corrections of all 383 P receiver functions for events with epicentral distances greater than 27° (Fig. 3). Move-out time corrections were calculated as *Ps* traveltimes for given depth of conversion in IASP91 model using the following formula:

$$t_{\text{moveout}} = t_{Ps}(D, p) - t_{Ps}(D, p_o), \quad (1)$$

where p, p_0 are slowness and reference slowness, respectively, D is conversion depth, t_{Ps} is the traveltime of converted *Ps* wave, with respect to P-wave onset. Standard earth model IASP91

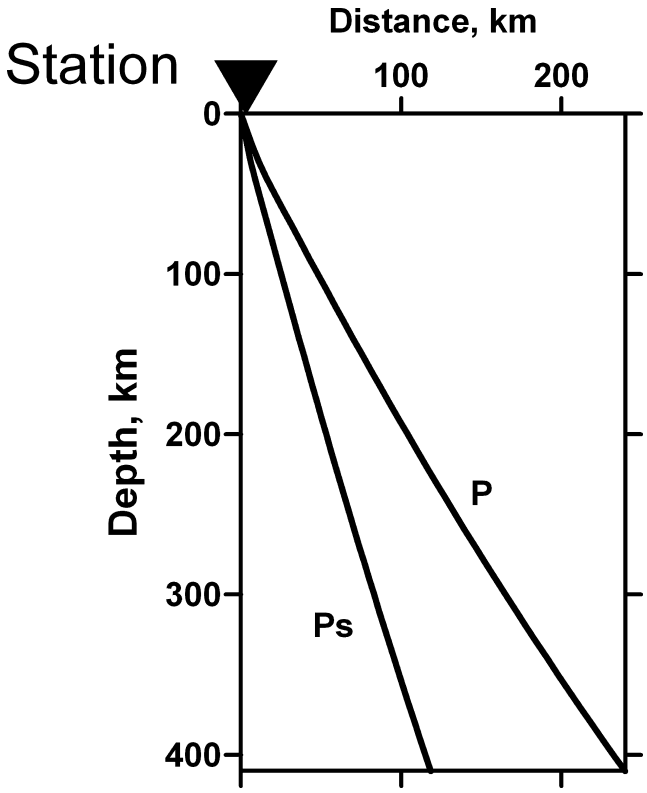

Figure 4. Figure showing position of piercing points of *P*-wave (denoted as *P*) and *Ps* wave (denoted as P_S) at the depth of 410 km (lower boundary of the plot).

and reference slowness $p_0 = 6.4$ s deg^{-1} were used for these calculations.

Fig. 3 shows clear focusing of converted phases at corresponding depths. The lowest trace in Fig. 3 is the sum of all 383 receiver functions. Therefore, the *Ps*410 and *Ps*660 traveltimes could be measured from Fig. 3 with good accuracy, and they are equal to 42.3 ± 0.1 and 66.2 ± 0.1 s, respectively. Thus, the traveltimes *Ps*410 and *Ps*660 for the SVEKALAPKO array are smaller by 1.8 s than the corresponding values for the standard earth model.

We calculated horizontal projections of piercing points at the depth of 410 km to the Earth's surface. These projections for *P* and *Ps* waves are shifted from the station position at about 240 and 120 km, respectively (Fig. 4). The value of Fresnel zone is about 100 km for the *Ps* wave converted at the depth of 410 km. As most of the earthquake epicentres (Table 1) are located east of the SVEKALAPKO array area, their conversion points are shifted eastwards. Despite this circumstance and taking into account the size of the Fresnel zone and rather large distance between conversion points and stations, we can assume that the region affecting propagation of the converted *Ps*410 and *Ps*660 waves includes the whole area beneath the SVEKALAPKO array. Therefore, traveltimes *Ps*410 and *Ps*660 can be assumed as average ones for the whole study area.

The difference between *Ps*660 and *Ps*410 traveltimes is equal to 23.9 s and it is in a perfect agreement with the standard IASP91 model. From this, one can conclude that the upper mantle beneath the SVEKALAPKO array is not anomalous at depths between 410 and 660 km and has higher velocities above 410 km only. We also calculated similar stacks for 15 separate stations and found minor differences in *Ps*410 traveltimes (1.5–2.5 s) at different stations of the array (Table 2). The stacks for other stations were too noisy; that is why we adopted the average *Ps*410 traveltime for them. An example of the stack of nine receiver functions for the station FJ01 is given in Fig. 5 .

Table 2. *Ps* delays for 410km discontinuity.

N	Station	τ_{PS} (s)
1	FA05	41.93
2	FB07	41.69
3	FB11	42.86
4	FC04	41.79
5	FD04	42.05
6	FD05	42.21
7	FD10	41.76
8	FD13	41.86
9	FE09	42.12
10	FF30	42.31
11	FF07	42.47
12	FF90	42.18
13	FF15	41.9
14	FJ01	42.87
15	FJ10	42.13
	Average	42.3

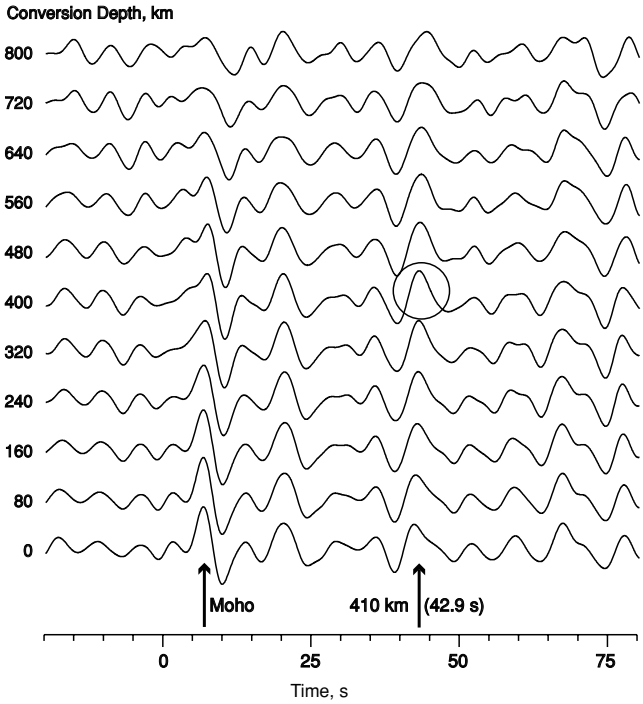

Figure 5. Stack of nine receiver functions for the station FJ01. Delay times of *Ps* conversions from the Moho boundary and 410 km discontinuity are indicated by arrows.

Following conclusions by Chevrot *et al.* (1999), we assumed in this paper that the depth of the 410 km discontinuity under all SVEKALAPKO stations (similarly as in the most other regions of the world) does not deviate significantly from 410 km.

2.3 Surface wave data

As mentioned above, additional data are required to stabilize inversion of receiver functions. Previousy, phase velocities of surface waves have been utilized for this purpose by Julia *et al.*

(2000). In this study, we use the phase velocities determined from SVEKALAPKO broad-band records by Bruneton *et al.* (2004a,b). They measured the traveltimes of the Rayleigh wave fundamental mode between their curvilinear fronts within the SVEKALAPKO array and inverted these data into the phase velocity field. A phase velocity curve in the range of periods from 10.5 to 190 s was constructed at every broad-band station of the SVEKALAPKO array. All these dispersion curves are presented in the paper by Bruneton *et al.* (2004b), who used them for calculation of the SVEKALAPKO surface wave tomography model. These data in the form of dispersion curves of the Rayleigh phase velocity at grid nodes covering the SVEKALAPKO array, were kindly provided to the authors by M. Bruneton. In our study, we used the range of periods from 10 s to 110 s.

3 INVERSION PROCEDURE

3.1 Model parametrization and constraints on model parameters

We modelled the medium under each station by a set of horizontal layers. The vector of model parameters **m** for each layer included *P*- and *S*-wave velocities, density and depth to the lower boundary of the layer. The way of the division into the layers is different in the crust and in the mantle. In our study, we used models consisting of 4–7 layers in the crust. Additional layer in the uppermost crust was introduced if a receiver function demonstrated presence of a sharp conversion within the first second from the *P*-wave arrival (see examples of receiver functions in Fig. 2).

The upper mantle in each 1-D model was modelled by a combination of a single layer and IASP91 model. Such a parametrization was based on characteristic features of the deep structure of the region. As demonstrated in previous body wave tomography and surface wave studies (Sandoval *et al.* 2004; Bruneton *et al.* 2004a,b), the upper mantle beneath the SVEKALAPKO array is laterally heterogeneous down to a depth of 300–350 km, where the velocities approach the values of the standard IASP91 model. However, the velocity anomalies are generally weak. The largest anomalies (about 2 per cent of IASP91 velocities) of a scale of 100–200 km are concentrated in the uppermost mantle down to a depth of 150–200 km (see Fig. 10 from Sandoval *et al.* 2004), whereas deeper anomalies are weaker than 1 per cent. Taking these results of previous studies into consideration, the upper mantle in each 1-D model was parametrized by a single layer, down to a depth of 300–350 km. From that depth and down to the depth of 410 km, we adopted the standard IASP91 velocity. This model was used to calculate the traveltime of the wave converted from the 410km boundary.

It should be noted that variations of velocities beneath 200–250 km have no influence on both receiver function and Rayleigh dispersion curves. Converted wave signals from depth more than 250 km arrive outside the time interval adopted in the study (from –5 to 25 s), and the surface waves with periods of 10–110 s sample the depth interval shallower than 200 km. Therefore, it is possible to use a simplified model for calculation of synthetic receiver functions and surface wave dispersion curves, in which the mantle is represented by a half-space.

To avoid the 'curse of dimension' (Tarantola 1987), we had to reduce the number of independent parameters. For this, we used the *a priori* information. The density in the crust was excluded from the parameters using the well-known statistical dependence between isotropic *P*-wave velocity and density in crustal rocks, approximated by some linear or non-linear equation (Birch 1961; Krasovsky 1981; Christensen & Mooney 1995). In our study, we used the equation by Krasovsky (Krasovsky 1981), as it is a good approximation of the relationship between density and *P*-wave velocity of crustal rocks in cold shield areas (Kozlovskaya *et al.* 2004b). However, this correlation does not hold for peridotitic rocks of the upper mantle. In cold cratonic lithospheric mantle, where the influence of temperature on rock density is minor compared with the effect of rock composition, the density of peridotitic rocks varies between 3.31 and 3.39 g cm^{-3} and depends mainly on degree of depletion in Fe (Griffin *et al.* 2003). We tested the effect of these density variations on inversion results using synthetic receiver functions and surface waves. Our estimation showed that such density variations have minor effect upon the inversion results compared with the effect of *S*-wave velocity. That is why, we assumed the constant density of 3.35 g cm^{-3} in the upper mantle.

Additionally, the following considerations were taken into account to decrease the number of model parameters and constrain the global search. As our data sets are more dependent on V_S than on V_P, we introduced the V_P/V_S parameter into inversion and constrained the values of V_P in the crust using the existing 3-D *P*-wave velocity models of the crust for the SVEKALAPKO area (Sandoval *et al.* 2003; Kozlovskaya *et al.* 2004a). The average values of *P*-wave velocity in each layer of 1-D models were taken from the model by Kozlovskaya *et al.* (2004a). To minimize the influence of artefacts that could be present in this model due to interpolation between profiles, we assumed that the V_P can vary around the average in a range of ± 0.5 km s^{-1}.

Second, we assumed a more rough segmentation for the V_P/V_S parameter than for the V_S. For this, we grouped the layers in the crust into several depth intervals. The first interval comprised the layers in the uppermost crust, down to the depth of about 30 km, whereas the layers below the depth of 30 km down to the Moho were united into the second group. This subdivision of the crust was based on results of study of V_P/V_S distribution in the crust and uppermost mantle by Janik *et al.* (2007). They analysed absolute values of V_P, V_S and V_P/V_S along two wide-angle reflection and refraction profiles located in the area covered by the SVEKALAPKO array and demonstrated that the major change of the V_P/V_S ratio in the crust occurs approximately at a depth of 30–35 km. This depth is roughly coincident with the depth of eclogite facies transition in the Fennoscandian Shield (Henkel *et al.* 1990). As shown by Janik *et al.* (2007), the composition of the crust changes at this depth either to mafic and mafic garnet granulites or to eclogites, resulting in sharp increase or decrease of V_P/V_S ratio, respectively.

Additional uppermost layer in the crust down to a depth of 1–2 km was introduced only if the evidence of low velocity layer in the uppermost crust was present in the receiver function. We also varied the V_P/V_S in the mantle. We assumed that the value of V_P/V_S is the same within each group, whereas between the groups, it varies independently, within the wide range of $1.6 < V_P/V_S < 1.8$.

3.2 Inverse problem formulation

Inversion procedure implies minimization of the functional

$$E(m) = \frac{1}{\sigma_{\mathrm{RF}}} \left\{ \frac{1}{t_2 - t_1} \int_{t_1}^{t_2} \left[Q_{\mathrm{syn}}(m,t) - Q_{\mathrm{obs}}(t) \right]^2 \mathrm{d}t \right\}^{1/2} + \frac{1}{\sigma_{\mathrm{Surf}}} \left\{ \frac{1}{T_2 - T_1} \int_{T_1}^{T_2} \left[R_{\mathrm{syn}}(m,T) - R_{\mathrm{obs}}(T) \right]^2 \mathrm{d}T \right\}^{1/2} + \frac{1}{\sigma_\tau} \left| \tau_{\mathrm{syn}}(m) - \tau_{\mathrm{obs}} \right|, \quad (2)$$

where $Q_{\rm obs}(t)$ is observed receiver function, $R_{\rm obs}(T)$ is measured dispersion curve for period T, $\tau_{\rm obs}$ is traveltime of the *Ps* wave converted at the 410 km boundary and $1/\sigma_{\rm RF}$, $1/\sigma_{\rm Surf}$, $1/\sigma_{\tau}$ are empirically chosen weights.

A synthetic receiver function $Q_{\rm syn}(\mathbf{m}, t)$ was calculated by the formula (Kind *et al.* 1995):

$$Q_{\rm syn}(m,t) = \frac{1}{2\pi}\int_{-\infty}^{\infty} \frac{H_Q(m,\omega)}{H_L(m,\omega)} L_{\rm obs}(\omega)\, {\rm e}^{{\rm i}\omega t}\, {\rm d}\omega. \qquad (3)$$

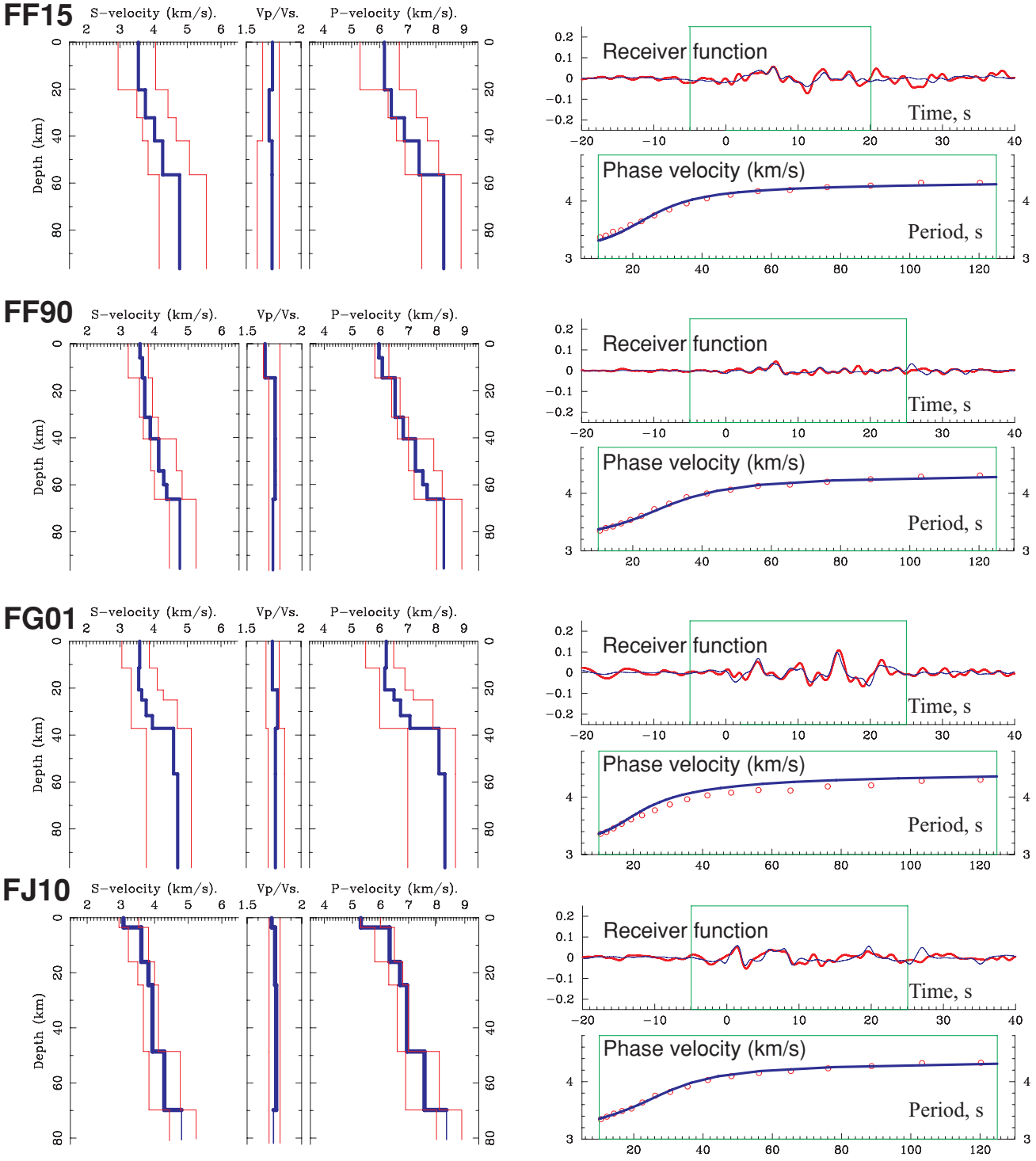

Figure 6. Examples illustrating model parametrization and inverse problem solution for four selected stations located in different geological units of the study area. Left-hand panel shows constraints on model parameters (red lines) and final 1-D models of the crust and upper mantle (blue lines). Right-hand panel shows fit of the synthetic receiver functions and phase velocity (shown by red colour) to the data (shown by blue colour). Green rectangles indicate parts of the receiver function and phase velocity used in the inversion.

The components of response of the layered medium $H_Q(\mathbf{m}, \omega)$ and $H_L(\mathbf{m}, \omega)$ were calculated by the Thomson–Haskell method (Haskell 1962). We select the time interval from –5 to 25 s for receiver function calculation to include the major converted phases.

Synthetic surface wave dispersion curve $R(\mathbf{m},T)$ was calculated by the code described by (Proskuryakova *et al.* 1981). The periods of 10–110 s were used.

We applied non-gradient global optimization techniques to find the solution to the minimization problem (2). First, the initial model was found using modification of the simulated annealing (SA) method (Ingber 1989). After that, a set of trial models was generated randomly, in the vicinity of initial model using Metropolis algorithm (Tarantola 1987). From this set, we selected the models, with the value of misfit function (2) less or equal to that of the initial model (total number of about 80 000–120 000) and calculated corresponding empirical *a posteriori* probability density functions (PDF) for each model parameter. The final solution was compiled from median values of these PDFs. Examples of model parametrization and inversion results for several selected stations are shown in Fig. 6.

As a result of inversion, we obtain a set of 1-D models for V_P, V_S, V_P/V_S ratio and density. However, these parameters are defined with different accuracy. It is known that both receiver functions and surface wave dispersion curves are more sensitive to changes of V_S at the boundaries than to the variations of V_P, and they are almost insensitive to density variations. Therefore, taking into account the nature of our experimental data and our model parametrization, we can conclude that our main result is a set of 1-D *S*-wave velocity models and V_P/V_S values in the groups of layers.

To prove the efficiency of the applied method and reliability of the results, we carried out several synthetic tests. First, we calculated synthetic receiver function for one of the obtained 1-D models (station FF15). Then we added random Gaussian noise, filtered according to the *L*-component spectrum to the synthetic receiver function (Fig. 7), and made an inversion exactly following the procedures we applied to the real data. The same procedure was repeated with the same synthetic data, but without *Ps*410 traveltime. Figs 8(a) and (b) show comparison of *a posteriori* PDF for both cases. The modelling showed that the traveltime of *Ps*410 phase has minor effect upon estimation of velocities and boundaries of layers, but it affects, strongly, determination of the V_P/V_S ratio. It is clearly seen (Fig. 8b) that ignoring data on *Ps*410 traveltime results in significant broadening of the PDF for V_P/V_S ratio and actually cancels the possibility of reliable estimation for the V_P/V_S parameter in the mantle, whereas taking into account the data on *Ps*410 traveltime results in narrowing and sharpening of the *a posteriori* PDF (Fig. 8) and the median value of the V_P/V_S in the mantle in this case is very close to the true one.

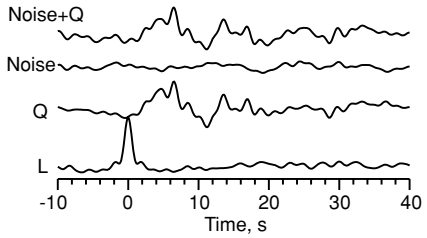

Figure 7. Example of a synthetic 'noisy' receiver function for the station FF15 used to test the efficiency of the inversion procedure. *L* denotes the *L*-component of receiver function, *Q* is synthetic *Q*-component of the receiver function. 'Noise' denotes the noisy trace produced as described in the text. 'Noise+*Q*' denotes the sum of last two traces, which was used in the inversion. The scale of the last three components is different compared with the scale of *L*-component.

The same numerical test was performed using real data for the FF15 station. We inverted receiver function together with the surface wave dispersion curve and with and without data on *Ps*410 traveltime (Figs 9a and b). Results of the test with real data confirm the effect of significant broadening of the *a posteriori* PDF for the V_P/V_S, in the case when traveltime of *Ps*410 was excluded from the inversion.

Numerical tests showed that the *Ps*410 traveltime had, practically, no influence on the results of V_S and V_P/V_S determination in the crust. This is due to the fact that both receiver function and surface wave dispersion data are very sensitive to variations of V_S; thus, introduction of *Ps*410 traveltime did not improve resolution for this set of parameters significantly. As we have imposed significant constraints on V_P values in the crust, the estimation of V_P/V_S in the crust was stable without the additional data set. Besides, we have introduced grouping of V_P/V_S in the crust, and it helped us to reasonably reduce the dimension of the inverse problem.

However, for the V_P/V_S distribution in the mantle, our numerical tests proved that reliable estimation of V_P/V_S in the mantle is possible only if the data on *Ps*410 traveltime is included into inversion. Compared with the crust, the *P*-wave velocities in the mantle were weakly constrained by the *a priori* information. In this case, inclusion of an additional data set helped to improve the resolution.

With respect to the V_P/V_S in the mantle, two options were also tested. At first, we found a solution, with the V_P/V_S in the mantle fixed to the value of 1.8. This value is often used as a 'standard' in receiver function studies, although it is generally valid only for hot regions. Inversion results showed, however, that such a value of V_P/V_S in the mantle results in over-estimated values of V_P (8.4–8.5 km s^{-1}), which do not agree with the values obtained by controlled-source seismic experiments in our study area. In the second test, the V_P/V_S value in the mantle was not fixed. It resulted in generally lower values of V_P/V_S in the mantle, which better agree with the values predicted from mantle xenolith data for cold cratonic mantle (Griffin *et al.* 2003). In this case, the estimates of V_P agree also well with the values obtained by wide-angle reflection and refraction experiments (Janik *et al.* 2007).

An example of 1-D velocity model beneath the station FJ01 is shown in Fig. 10, where it is compared to the global IASP91 model, as well as to the average regional *S*-wave velocity model for the SVEKALAPKO area by Bruneton *et al.* (2004a) and to the *S*-wave velocity in the mantle, estimated from xenoliths data (Kukkonen *et al.* 2003). It is seen that the model is substantially different from the IASP91 model concerning structure of the crust and uppermost mantle down to a depth of 250 km. The model agrees well with the xenoliths data and with the regional *S*-wave velocity model obtained by surface wave studies, although certain differences from the regional model can be distinguished for this separate station.

4 RESULTS

4.1 The Moho boundary

To define the depth to the Moho boundary from 1-D velocity models, we used the following criteria, selected on the basis of analysis of *P*- and *S*-wave velocity models of previous wide-angle reflection and refraction profiles (Janik *et al.* 2007): (a) the V_P should be more than 8.0 km s^{-1} and (b) the V_S should be more than 4.5 km s^{-1}. Then, the

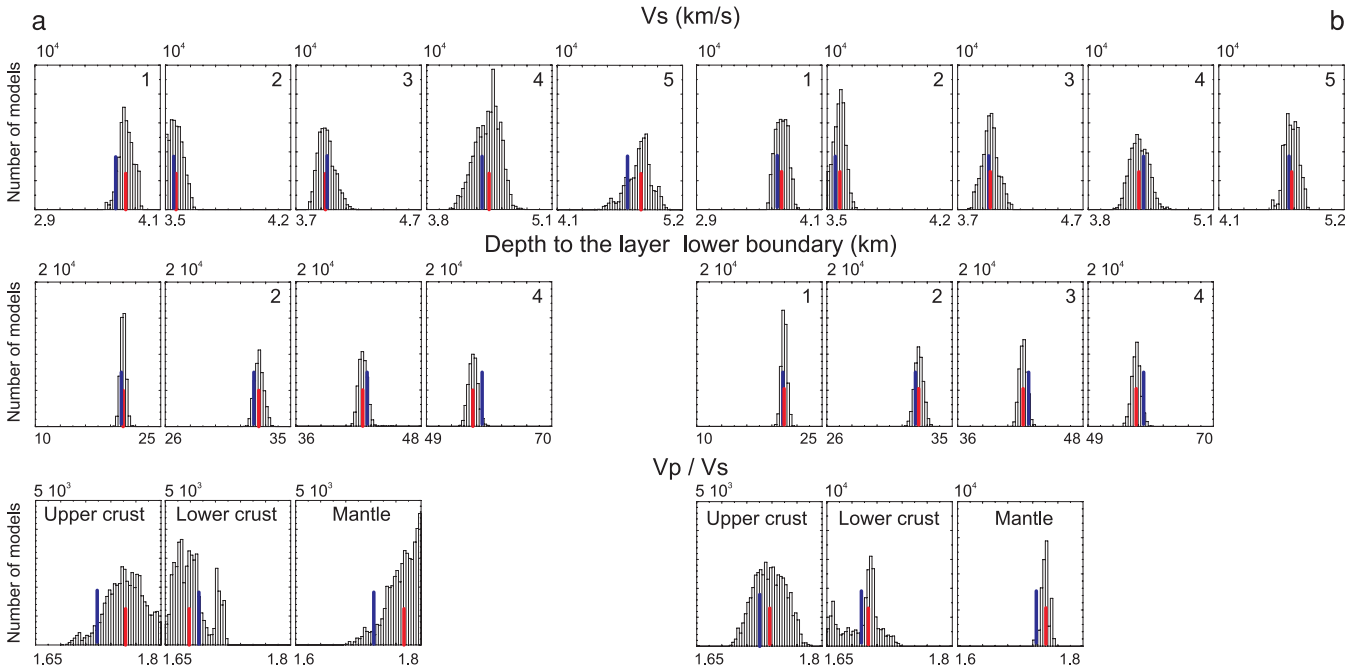

Figure 8. *A posteriori* PDF obtained after inversion of synthetic data. (a) PDF for *S*-wave velocities, depths to the lower boundary of layers, and V_P/V_S obtained without traveltime *Ps*410; (b) the same as (a) when traveltime *Ps*410 was included into inversion. Red line marks median of the PDF and blue line marks the true solution.

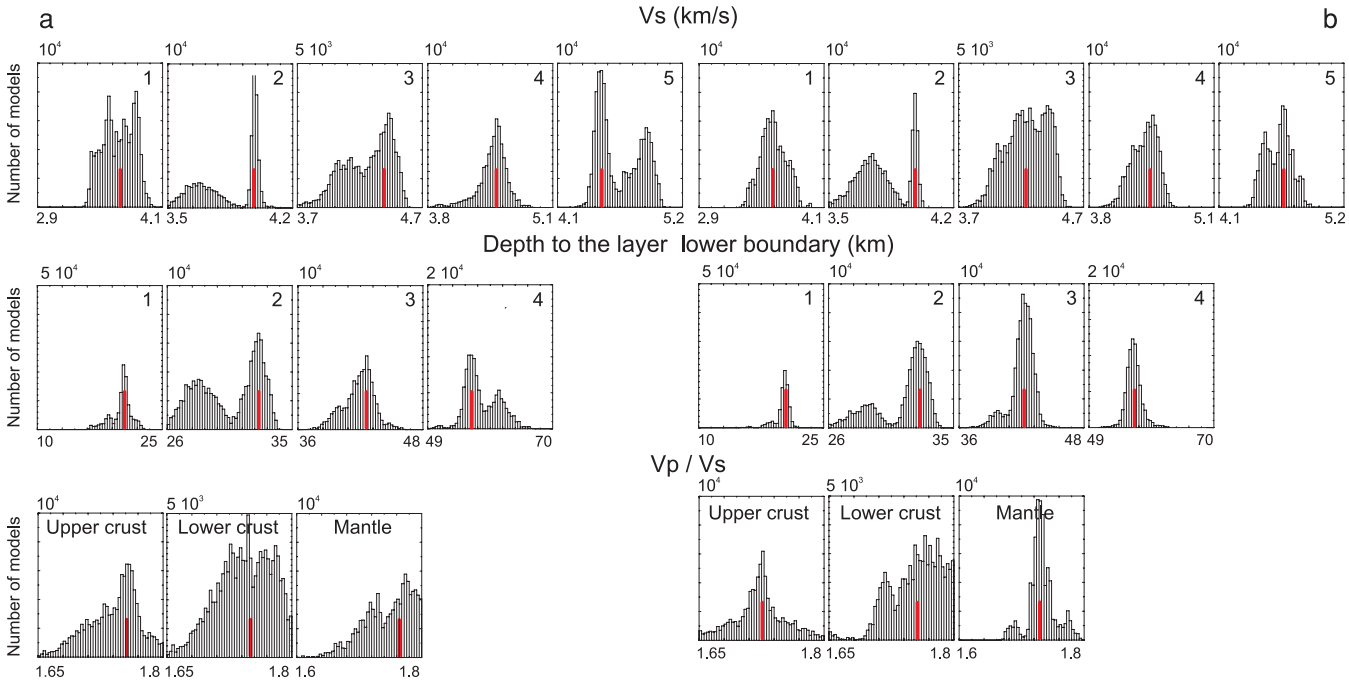

Figure 9. *A posteriori* PDF obtained after inversion of real data of station FF15. (a) PDF for *S*-wave velocities, depths to the lower boundary of layers and V_P/V_S obtained without traveltime *Ps*410; (b) the same as (a) when traveltime *Ps*410 was included into inversion. Red line marks median of the PDF.

depths to the Moho boundary beneath all stations were interpolated into a regular, grid using Kriging technique. The crustal thickness map is shown in Fig. 11.

Generally, our result shows no correlation between the Moho depth and the age of major tectonic units observed on global scale (Christensen & Mooney 1995). Compared with the previous Moho maps obtained by interpolation of existing profiles (Luosto 1997; Sandoval *et al.* 2003), the area with the crustal thickness of more than 50 km is larger, and such deep Moho is seen beneath both Archean and Proterozoic terrains. The maximum crustal thickness of 64 km occurs beneath the Proterozoic Central Finland Granitoid Complex (CFGC), which agrees with the result by Alinaghi *et al.* (2003) and Janik *et al.* (2007). A narrow trough, with crustal thickness up to 52 km, stretches beneath the Archean domain from

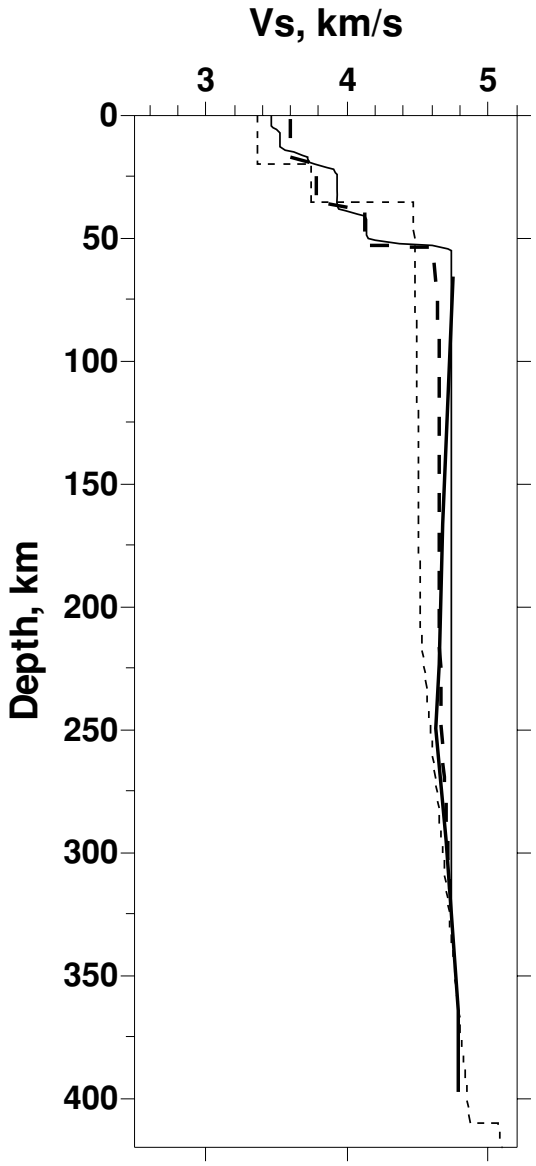

Figure 10. 1-D *S*-wave velocity model obtained at the station FJ01. The IASP91 standard model is shown by thin dashed line. The 1-D velocity model calculated from xenoliths data (Kukkonen *et al.* 2003) is shown by thick solid line. Thick dashed line shows the model based on surface wave data (Bruneton *et al.* 2004) and thin solid lines shows the model obtained in this study.

the main maximum and becomes shallower (48 km on average) to the north. Deep Moho in this part of the Karelian domain has been detected previously by Yliniemi (1991). The shallowest Moho is observed beneath the Late Proterozoic Wyborg rapakivi massif (WRM) and also to the east of the Archean Kuhmo greenstone belt.

4.2 *S*-wave velocity model

To obtain a 3-D velocity model from the individual 1-D velocity models, we used method described by Vinnik *et al.* (2004). Each individual 1-D model was smoothed with a Gaussian filter, with standard deviation of 1 km. Then the velocity values from 1-D models were taken at every 1 km in a depth range of 0–75 km. The corresponding velocity values at any given depth were interpolated to regular 2-D grids with the standard Kriging technique (Isaacs & Srivastava 1989). The points of vertical sections through the 3-D model were obtained using linear interpolation.

4.2.1 S-wave velocity distribution in the crust

Fig. 12 shows horizontal cross-sections through the 3-D velocity model and Fig. 13 shows vertical cross-sections of the *S*-wave velocity model along selected lines shown in Fig. 1.

Generally, Archean granitoids, Proterozoic CFGC and Wyborg rapakivi batholith have higher *S*-wave velocities, whereas Proterozoic shists and migmatites have lower *S*-wave velocities in the upper crust (Figs 12a and b).

One of the interesting features revealed by our study is a thin layer (down to 2 km) of low *S*-wave velocity in the uppermost crust, which is seen at several stations (Fig. 12a). The same layer was revealed also beneath APA and LVZ stations in the Kola Peninsula (Dricker *et al.* 1996) and beneath RUKSA array (Aleshin *et al.* 2006). The layer has not been revealed either by previous controlled-source experiments or by local event studies based on body waves (Hyvönen *et al.* 2007), although this layer has been indicated by the analysis of surface waves from quarry blasts and shots registered during the SVEKA wide-angle refraction and reflection experiment (Pedersen & Campillo 1991; Grad & Luosto 1994). Thus, the ability to reveal such layers can be considered as an important advantage of joint inversion of surface waves and receiver functions compared with local event tomography. The stations, where this layer was detected, are located within the Kainuu schist belt (KaB) and the Svekofennian shists and vulcanites. Therefore, low *S*-wave velocity values in this layer can be explained by micro- and macrofracturing. The other station, where this layer is present (FD13), is situated to the west of the Wyborg rapakivi batholiths (WRM). Surprisingly, this layer is not seen at the station FF15, although stations FD13 and FF15 belong to the same geological unit (Fig. 1). Difference in crustal velocity structure between these two stations can be followed down to a depth of 30–40 km (Fig. 12). Janik *et al.* (2007) suggested that there should be an unexposed terrain boundary stretching NS and located approximately between these stations.

In the middle crust (Fig. 12c), we can see a number of high and low velocity heterogeneities; however, no direct correlation with the surface geology can be seen. At a depth of 30 km (Fig. 12d), the most pronounced feature is a zone of high *S*-wave velocities that stretches NS below the Outokumpu area (OA) and between Kuhmo greenstone Belt (KuB) and Kainuu Shist Belt (KaB). It is spatially coincident with the area of deep Moho and it is still seen at a depth of 38 km (Fig. 12e). Relatively high *S*-wave velocity is seen also beneath the western part of the CFGC at a depth of 30 km, although it should be interpreted with caution, as it has been detected at one station only.

As can be concluded from Figs 12 and 13, the high-velocity lower crust (HVLC) with $V_S > 4.1$ km s^{-1} was detected beneath many stations of the SVEKALAPKO array considered in our study. There is a good correlation between thickness and velocity structure of this layer and results of previous controlled-source experiments in the places where these profiles intersect our interpolated 3-D model.

In previous studies based upon interpretation of *P*-waves, this layer was considered as a homogeneous one, resulting from magmatic under- and intraplating in Proterozoic (Korja *et al.* 1993; Korsman *et al.* 1999). Recently Janik *et al.* (2007) demonstrated,

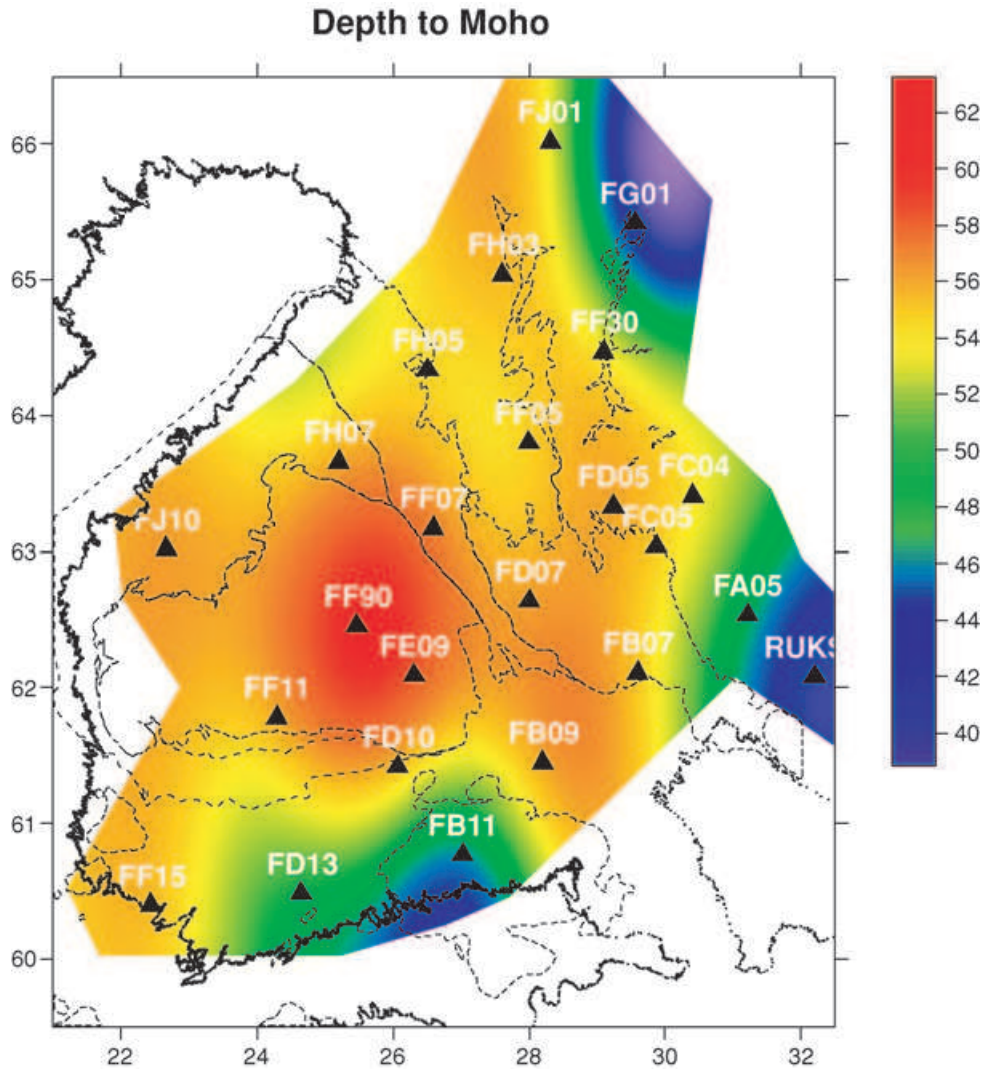

Figure 11. Map of the depth to the Moho boundary (in km). Broad-band stations of the SVEKALAPKO array and RUKSA small-apreture array are shown by black triangles. Position of geological units shown in Fig. 1 is indicated by thin dashed lines.

however, that this layer is laterally and vertically inhomogeneous, because *P*-wave velocities and, in particular, V_P/V_S ratio differ significantly within it. Janik *et al.* (2007) proposed that this can be explained by multigenetic origin of the HVLC and the Moho boundary in our study area. They distinguish the HVLC composed of mafic garnet granulites, formed as a result of magmatic underplating and/or re-melting of the old lower crust (with V_P/V_S ratio of 1.76–1.77) from the HVLC composed of rocks that underwent transition to eclogite phases (with V_P/V_S ratio of 1.73–1.74). Signatures of these two types of the HVLC can be seen also in the crustal model by Hyvönen *et al.* (2007), although their model reaches the depth only to 40 km.

As can be seen in Figs 8 and 9, the value of the V_P/V_S in the lower crust is not well resolved by our data set. However, the values of V_P/V_S in the HVLC revealed by our study can be roughly subdivided into the same two groups (Fig. 14), namely, low V_P/V_S, corresponding to eclogitized rocks, and high V_P/V_S, corresponding to magmatic underplating and re-melting of the old crust. Spatial distribution of these two types of HVLC is generally in a good agreement with the result by Janik *et al.* (2007) and Hyvönen *et al.* (2007). Thus, together with other studies, our result supports multigenetic origin of the HVLC in the contact zone between Archean and Proterozoic domains.

4.2.2 S-wave velocity and V_P/V_S distribution in the upper mantle

Estimates of V_P/V_S ratio by wide-angle reflection and refraction techniques demonstrated that V_P/V_S in the crust varies significantly with depth (see, for example, Musacchio *et al.* 1997; Korsman *et al.* 1999; Janik *et al.* 2007). In spite of this, it is now widely accepted in receiver function studies to estimate and interpret lateral variations of the average value V_P/V_S ratio in the crust using technique by Zhu & Kanamori (2000). Although such models do not represent the true 3-D distribution of V_P/V_S ratio in the crust and can be treated as a first-order approximation only, they can be used to infer major compositional differences between various tectonic units of the crust (Alinaghi *et al.* 2003; Eaton *et al.* 2006; Lombardi *et al.* 2006). In our study, we estimated lateral variations of upper-mantle velocities (V_S, V_P and V_P/V_S) averaged over the depth from the Moho boundary to 200 km (Fig. 15). Similarly to the average velocity distribution in the crust used in conventional receiver function studies, this model represents a first-order approximation of a true distribution

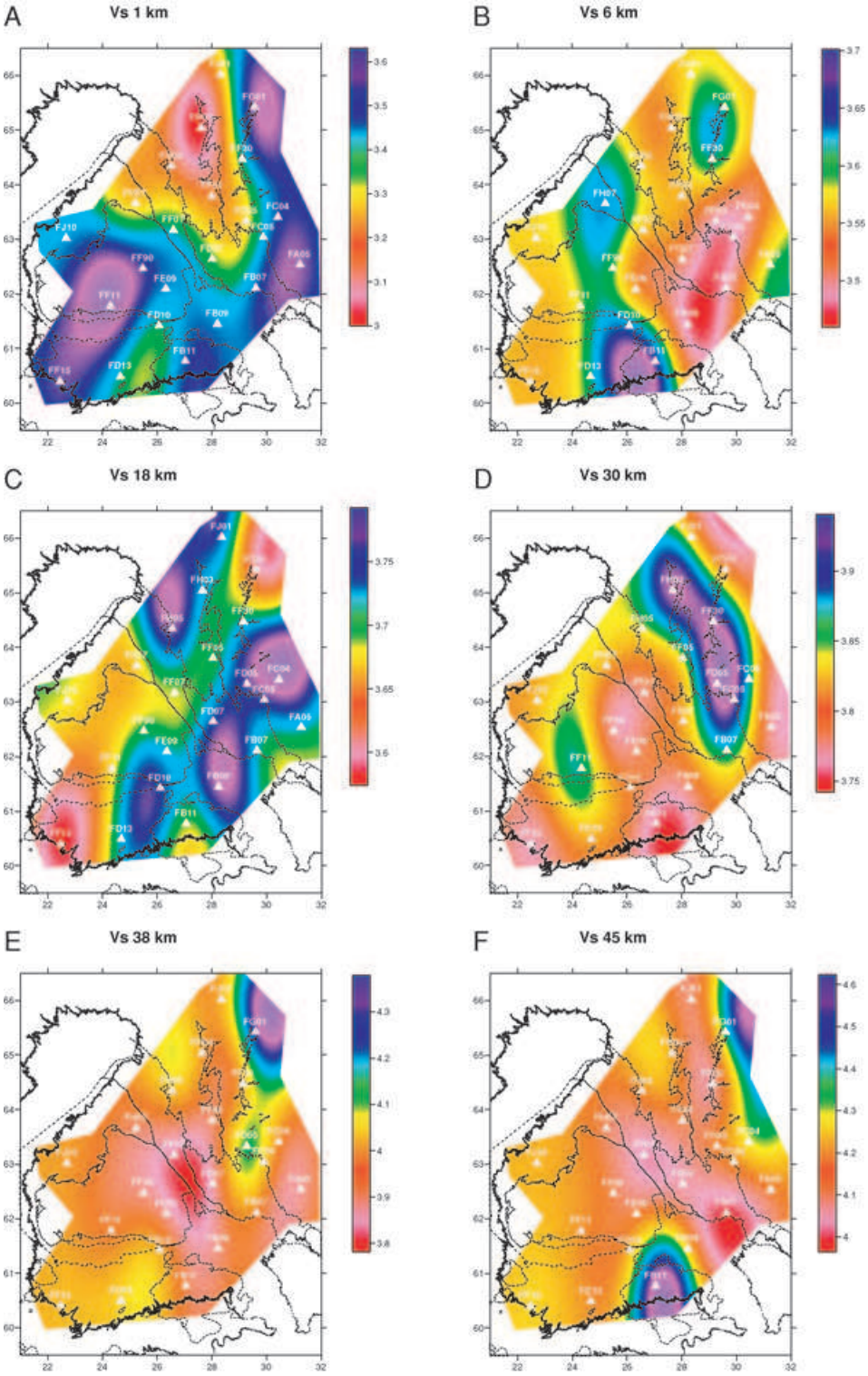

Figure 12. Horizontal cross-sections of *S*-wave velocity model at different depths obtained by interpolation of 1-D velocity models. *S*-wave velocity in km s^{-1} is shown by colour scale. Thin dashed lines indicate position of major geological units shown in Fig. 1. The broad-band stations of the SVEKALAPKO array are shown by white triangles.

of seismic velocities in the mantle. Therefore, it can be used to infer major differences in upper-mantle composition beneath our study area.

It is seen that *S*-wave velocities in the upper mantle are rather similar at the most of the stations. Only two stations in the Proterozoic domain (FJ10 and FF11) have velocities lower than 4.6 km s^{-1}. At other stations, the *S*-wave velocity varies from 4.7 to 4.75 km s^{-1} in the central part of the array. Similar values were obtained by Griffin *et al.* (2003), by analysis of xenolith samples from Archean SCLM around the world. These velocities agree with the values estimated

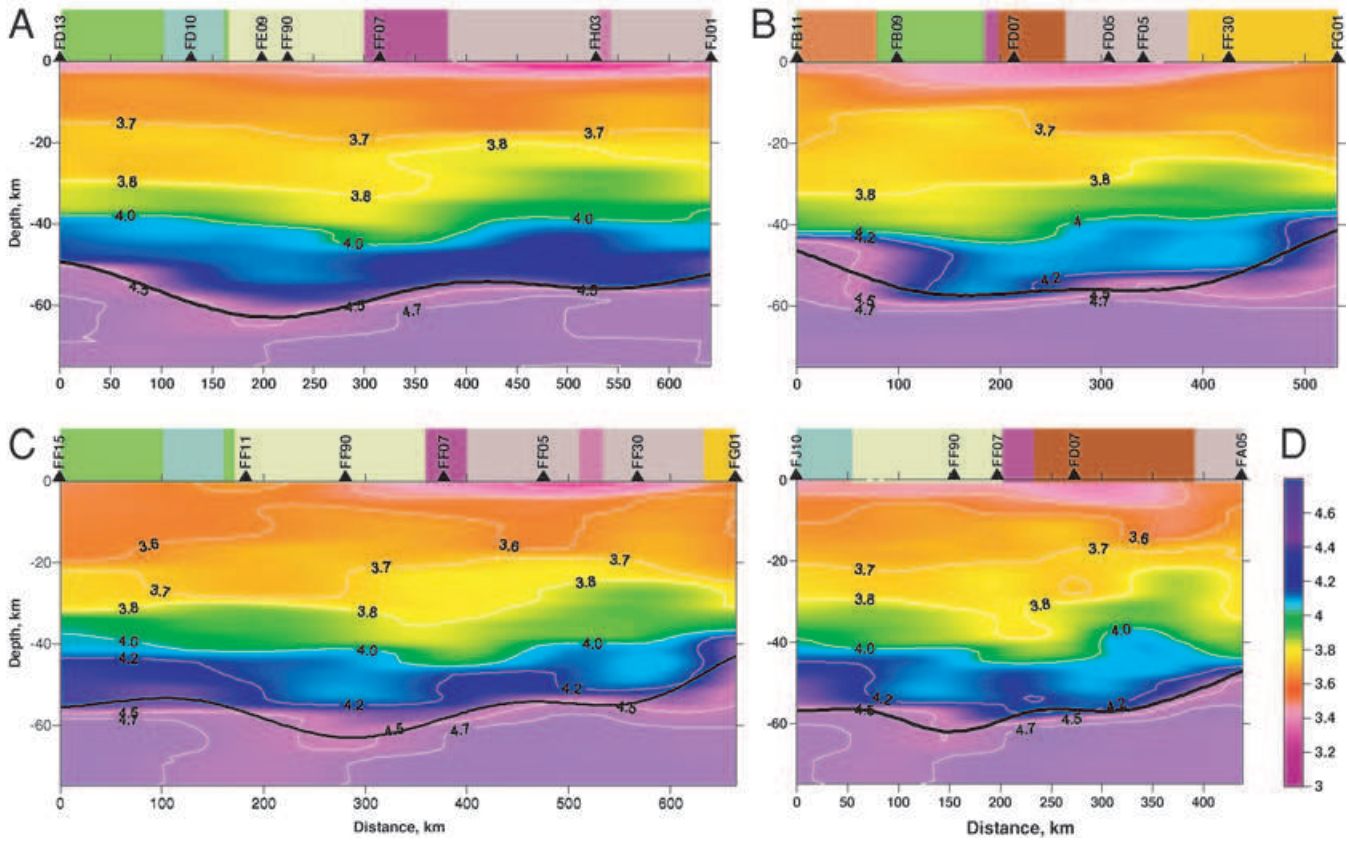

Figure 13. Vertical cross-sections through the 3-D *S*-wave velocity model along four selected profiles. *S*-wave velocity in km s^{-1} is shown by colour scale. Position of profiles in the study area is shown in Fig. 1. Rectangle above each profile indicates position of major geological units, which are shown by the same colours as in Fig. 1.

from highly depleted lherzolite and harzburgite xenoliths from eastern Finland that contain about 70 per cent of olivine with a high Mg/(Mg+Fe) ratio of about 0.9 (Kukkonen *et al.* 2003; Bruneton *et al.* 2004a). The simplest explanation of these minor differences in *S*-wave velocities can be different degree of depletion in Fe. This straightforward interpretation cannot be accepted, however, because distribution of V_P and V_P/V_S is more heterogeneous, and values of these parameters are substantially higher than those typical for peridotitic mantle (Griffin *et al.* 2003; Kukkonen *et al.* 2003) beneath several stations (Fig. 15). Such a combination of V_P and V_P/V_S ratio can indicate either eclogitic composition or seismic anisotropy (Kobussen *et al.* 2006), although additional evidence is necessary to distinguish between these two explanations.

P- and *S*-wave velocities lower than 8.0 and 4.6 km s^{-1}, respectively, and V_P/V_S ratio of 1.78 are observed at the station FJ10, located in the Pohjanmaa area (PoB). These values suggest that upper mantle there is contaminated by lower crustal material that was brought to the mantle during subduction processes in Proterozoic and partly transformed to eclogites. This agrees with recent results of FIRE3 reflection profile that revealed a series of inclined reflectors beneath PoB, penetrating through the whole crust into the upper mantle (Kukkonen *et al.* 2006). Similar low values of V_P beneath this unit have been revealed also by Yliniemi *et al.* (2004).

Low *S*-wave velocity, but relatively high V_P/V_S ratio was revealed beneath the station FF11 located in the CFGC. Similar values of V_P, V_S and V_P/V_S in the upper mantle of the CFGC were revealed also by Janik *et al.* (2007). They argued that high V_P/V_S ratio due to low V_S suggests eclogitic composition of the upper mantle there. The anisotropy in the upper mantle beneath these two stations is weak (Vecsey *et al.* 2007); thus, compositional variation is more plausible explanation of high V_P/V_S values.

High values of V_P and V_P/V_S ratio were revealed also beneath the WRM. As emplacement of 1.6–1.2 Ga anorogenic rapakivi granites and anorthosites was the last tectonothermal event there, these values can be hardly explained by seismic anisotropy because any previous frozen-in anisotropy would be destroyed. Thus, they may correspond to magmatic mafic rocks, like olivine gabbro reported in the study by Sobolev & Babeyko (1994). Similar high V_P/V_S ratios were revealed in the upper mantle in the vicinity of the Korosten rapakivi-anorthosite massif in the Ukrainian Shield (Bogdanova *et al.* 2006).

Stations FC04 and FA05 in the Archean domain have values of V_P, V_S and V_P/V_S that are typical isotropic velocities, revealed by studies of peridotitic xenoliths from Archean areas. This suggests that the mantle beneath these stations represents highly depleted Archean mantle (Griffin *et al.* 2003). In the Proterozoic domain, similar values of V_P/V_S, but slightly higher values of V_P are revealed beneath the stations FD13, FE09, FF90, FD10, FH07. They can indicate peridotitic composition, as anisotropy in this area is low (Vecsey *et al.* 2007).

The rest of stations show higher *P*-wave velocities and higher V_P/V_S ratios than the values typical for upper-mantle peridotites. They are located mainly within the Archean domain, where studies by Plomerova *et al.* (2006) and Vecsey *et al*. (2007) revealed strong seismic anisotropy. It should be remembered, however, that these studies could not evaluate the depth, from which the anisotropy

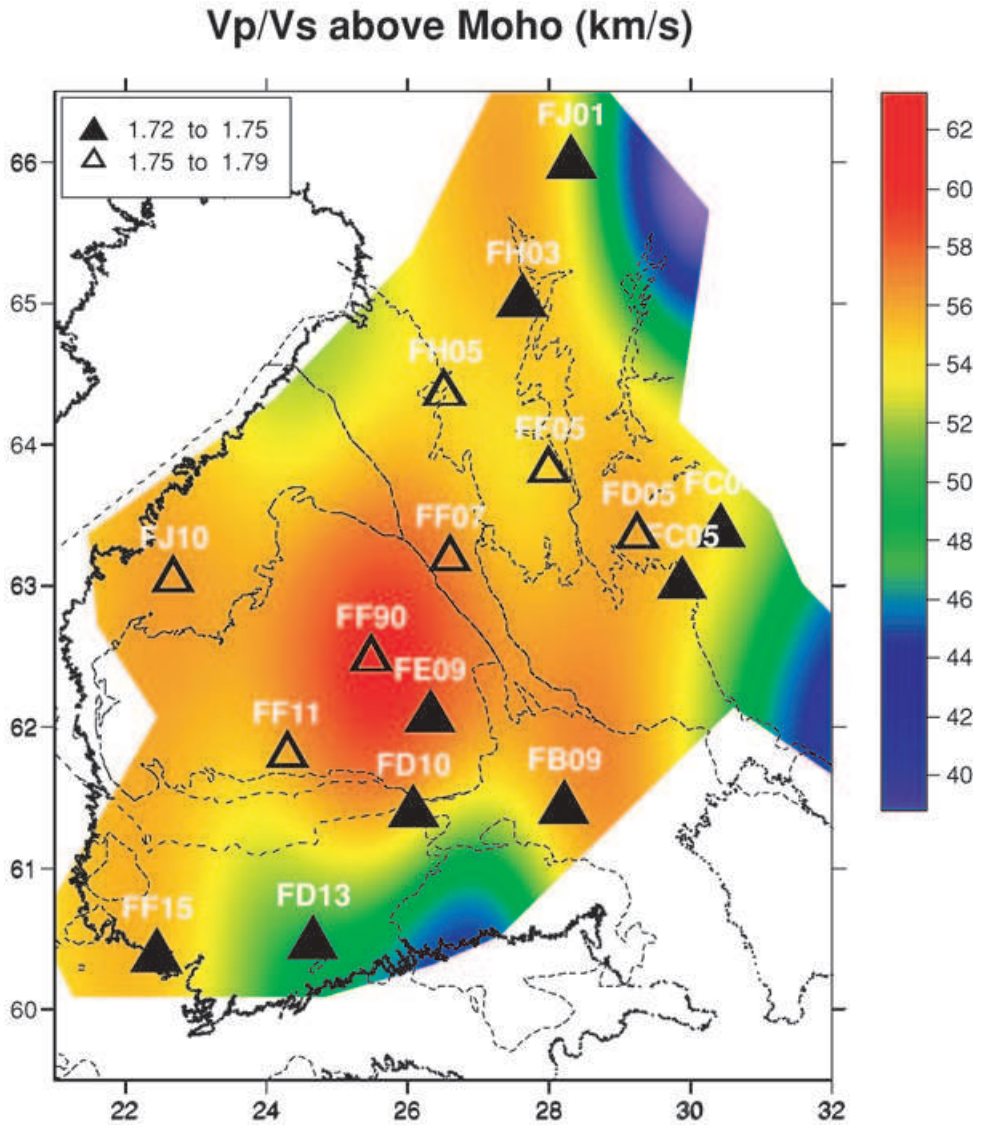

Figure 14. V_P/V_S ratio at the bottom of the high-velocity lower crust, superimposed on the depth to the Moho boundary (in km, shown by colour scale). Position of major geological units from Fig. 1 is indicated by dashed lines. Two ranges of values of V_P/V_S ratio at correspondent stations are shown by black and empty rectangles, respectively. Only stations where the HVLC was detected are shown.

originates. That is why our model is not directly comparable to their results. Another investigation of the upper-mantle anisotropy based on surface waves (Pedersen *et al.* (2006) has better depth resolution than the methods based on body waves, but it gave only the average anisotropy beneath the array. Thus, we cannot distinguish between two possible explanations of these high V_P and V_P/V_S values in the upper mantle.

5 DISCUSSION

Models of the assembly history of the Fennoscandian Shield involve extensive collisional accretion of island arcs and microcontinental blocks (Lahtinen *et al.* 2005). Such accretionary processes may be expected to produce a complicated mosaic of varying Moho structures and variety of crustal and mantle lithologies. Our study supports this hypothesis and shows that these processes were working both in Archean and Proterozoic time. Generally, we don't see correlation between crustal structure and tectonothermal age of Proterozoic and Archean crustal terrains or systematic difference between upper-mantle structure of Archean and Proterozoic domains.

Earlier it was proposed (Korsman *et al.* 1999) that the major Archean–Proterozoic suture (so-called Ladoga-Bothnian Bay Zone) is stretching SE–NW and roughly can be associated with the Savo Belt (Fig. 1). Our study shows that this structure is not observed as a mega-suture in the crust and upper mantle. Instead, our study demonstrated that the mega-scale suture zone separating typical Archean and Proterozoic lithospheres is broader, and it is limited from the east by the Kuhmo greenstone belt. This transitional zone can be associated with the 'Moho trench' stretching to the North from the OA along the KaB and KuB. The trench is spatially coincident with a zone of high V_P/V_S and high V_P in the mantle. To the east of this zone, we observe typical thin and felsic Archean crust (Fig. 11), which is very close to the global average for Archean areas (Christensen & Mooney 1995), no well-developed HVLC (Figs 12 and 13) and depleted peridotitic upper mantle (Fig. 15). To

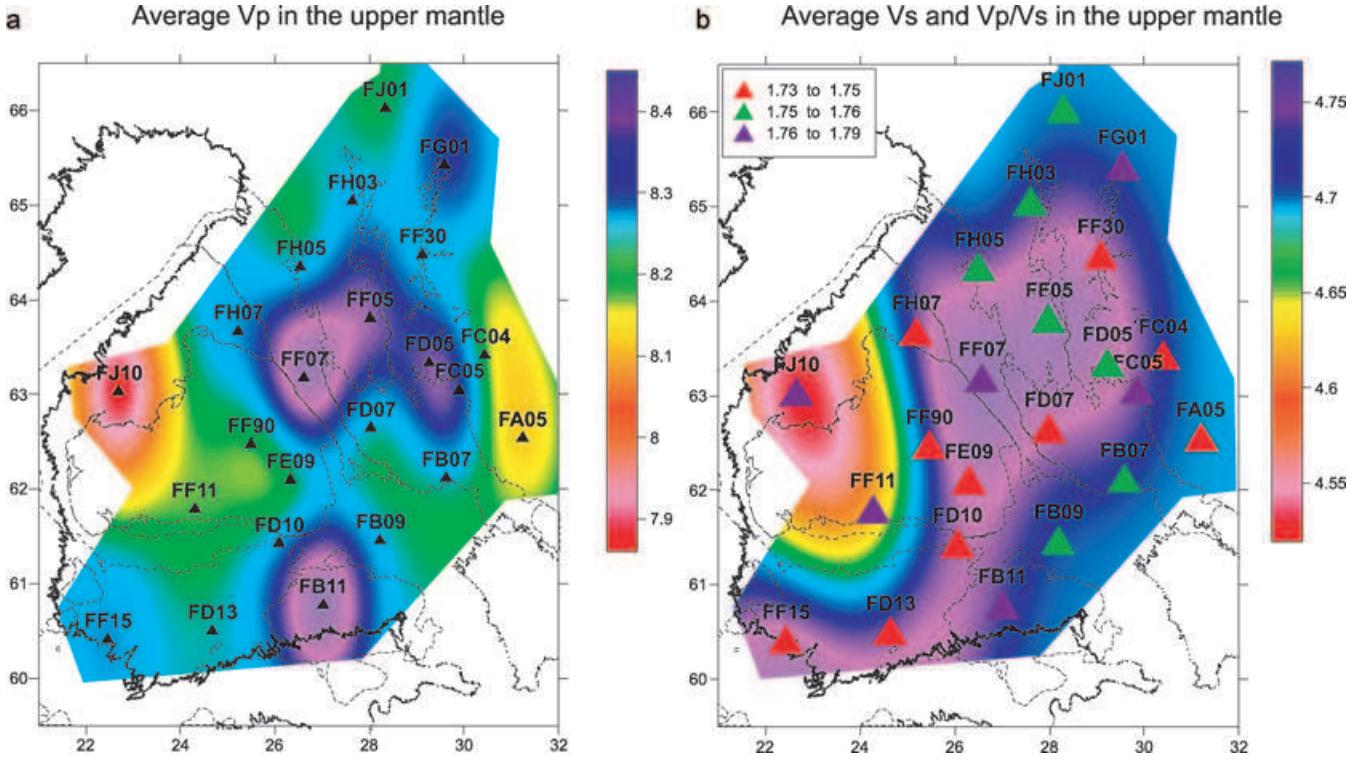

Figure 15. (a): Averaged *P*-wave velocity in the uppermost mantle (depths: 66–72km); (b) Averaged *S*-wave velocity and V_P/V_S ratio in the uppermost mantle. Velocities in km s^{-1} are shown by colour scale. Different values of V_P/V_S ratio at correspondent stations are shown by coloured triangles. Position of major geological units from Fig. 1 is indicated by dashed lines.

the west of it, beneath the CFGC and PoB, we observe thick crust, with properties resembling typical Proterozoic crust (Christensen & Mooney 1995), and generally peridotitic upper mantle, but with signatures of subduction and collision processes resulting in eclogitic composition of upper mantle beneath some stations. The HVLC with high V_P/V_S ratio there was formed as a result of magmatic underplating.

No typical Archean or Proterozoic structure of the crust and upper mantle is observed beneath the transitional zone. Although it is located in the Archean domain, to the east from the exposed Archean–Proterozoic suture, it has very thick crust and a HVLC. In addition, this zone has high V_P and high V_P/V_S ratio in the upper mantle, which are not observed in adjoining areas. Although we cannot distinguish whether such high values are due to seismic anisotropy or eclogitic composition, both these explanations suggest that this zone was formed as a result of plate-tectonic processes. This agrees also with the recent study by Silvennoinen & Kozlovskaya (2007), who demonstrated that the Kuhmo greenstone belt most probably was formed as a result of plate-tectonic processes.

At present, there is no tectonic model capable to explain the evolution of this area. Although evolution of the Proterozoic Svekofennian domain has been discussed in numerous studies (*cf*. Korsman *et al.* 1999; Lahtinen *et al.* 2005), the evolution of Archean Karelian craton is still unclear. It has been suggested that the Proterozoic Kainuu Shist belt was implaced into Archean crust as a result of rifting of the Karelian Craton in Proterozoic (Korja *et al.* 2006). However, Peltonen *et al.* (2006) demonstrated that the crust beneath this unit and its surrounding was very thick (about 50 km), already in Archean. Thus, rifting of such a thick crust in Proterozoic is hard to explain.

Together with other results of the SVEKALAPKO project, our study shows that evolution of the western margin of the Karelian Craton was probably more complicated than it was supposed before. It is not clear how this transitional zone continues outside the area of the SVEKALAPKO array. We hope that new lithosphere studies in the Fennoscandian Shield can help to answer this question.

6 CONCLUSIONS

(1) The new 3-D seismic models demonstrate pronounced lateral variations of values of V_S and V_P/V_S ratio in the crust and upper mantle and of the depth to the Moho boundary. The depth to the Moho boundary varies from 51 to 63 km, which agrees with the results of previous controlled-source seismic studies in the region and previous receiver function studies.

(2) The Moho boundary is overlain by a high-velocity lower crust (HVLC) with $4.05 < V_S < 4.23$ km s^{-1}, which is non-uniform in composition and origin.

(3) Low velocity layer in the uppermost crust (1–2 km) has been revealed within the Kainuu schist belts and Svekofennian shists and vulcanites.

(4) Our study confirms results of the SVEKALAPKO teleseismic body wave tomography and surface wave studies that showed no correlation between crustal structure and tectonothermal age of Proterozoic and Archean crustal terrains exposed at the surface.

(5) Earlier proposed Archean–Proterozoic suture exposed at the surface is not observed as a mega-suture in the crust and upper mantle.

(6) Our study suggests that the transition zone between Archean and Proterozoic lithosphere is broad and stretches to the North

along the Proterozoic Kainuu Shist Belt and the Archean Kuhmo greenstone belt.

(7) Our study supports the theory that the Fennoscandian Shield was assembled as a result of extensive collisional accretion of island arcs and microcontinental blocks and suggests that these processes were working both in Archean and Proterozoic.

ACKNOWLEDGMENTS

We appreciate very much fruitful comments of two anonymous reviewers, which helped us to improve the earlier version of the manuscript. We are grateful to M. Bruneton, who kindly provided us with data on phase velocities of surface waves. Visits of I. M. Aleshin and G. L. Kosarev to Oulu University, in 2004 and 2006, at the invitation of E.K. were supported by research grants No. 208069 and No.112975, respectively, of The Academy of Finland. Experimental observations with the RUKSA array were supported by the INTAS grant 97-0936 and the Zurich ETH Institute (Switzerland). This work was supported by the Russian Foundation for Basic Research, projects nos. 03-05-64654, 04-05-64634, 04-07-90362-B, 07-07-12031-ofi and 08-07-12108-ofi. The assistance of Dr T. Korja from the Department of Geophysics of Oulu University, who provided materials for a geological map of the area, is highly appreciated. SVEKALAPKO field experiment was organized by Geophysical Institute of CAS (Czech Republic); GFZ Potsdam and University of Stuttgart (Germany); University of Oulu and University of Helsinki (Finland); University of Grenoble and University of Strasbourg (France); Utrecht University (Netherlands); Kola Scientific Center RAS in Apatity, Institute of the Physics of the Earth, Moscow, St. Petersbourg University, Spetzgeofisika MNR Moscow (Russia); Warsaw University and Institute of Geophysics of PAS (Poland); University of Uppsala (Sweden) and Institute of Geophysics, ETH Zurich (Switzerland). The SVEKALAPKO Seismic Tomography Working Group consists of U. Achauer, A. Alinaghi, J. Ansorge, G. Bock, M. Bruneton, W. Friederich, M. Grad, A. Guterch, S.-E-. Hjelt, T. Hyvönen, E. Isanina, J.-P. Ikonen, E. Kissling, K.Komminaho, A. Korja, P. Heikkinen, E. Kozlovskaya, M.V. Nevsky, N. Pavlenkova, H. Pedersen, J. Plomerova, T. Raita, O. Riznichenko, R.G. Roberts, S. Sandoval, I.A. Sanina, N.V. Sharov, J. Tiikkainen, S.G. Volosov, E. Wieland, K. Wyegalla, J. Yliniemi and Y. Yurov.

REFERENCES

Aleshin, I.M., Kosarev, G.L., Riznichenko, O.Yu. & Sanina, I.A., 2006. Crustal velocity structure under the RUKSA seismic array (Karelia, Russia), *Russian J. Earth Sci.,* **8,** ES1003, doi:10.2205/2006ES000194.

Alinaghi, A., Bock, G., Kind, R., Hanka, W., Wylegalla, K & TOR and SVEKALAPKO Working Groups, 2003. Receiver function analysis of the crust and upper mantle from the North German Basin to the Archaean Baltic Shield, *Geophy. J. Int.,* **155,** 641–652.

Ammon, C.J., 1990. On the nonuniqueness of receiver function inversions, *J. geophys. Res.,* **95,** 2504.

Ammon, C. J., Randall, G. E. & Zandt, G., 1990. On the non-uniqueness of receiver function inversions, *J. geophys. Res.,* **95,** 15303–15318.

Artemieva, I., 2006. Global $1^\circ \times 1^\circ$ thermal model TC1 for the continental lithosphere: implications for lithosphere secular evolution, *Tectonophysics,* **416,** 245–277.

Artemieva, I.M. & Mooney, W.D., 2001. Thermal structure and evolution of Precambrian lithosphere: a global study, *J. geophys. Res.,* **106,** 16 387–16 414.

Artemieva, I.M. & Mooney, W.D., 2002. On the relation between cratonic lithosphere thickness, plate motions, and basal drag, *Tectonophysics,* **358,** 211–231.

BABEL Working Group, 1990. Evidence for early Proterozoic plate tectonics from seismic reflection profiles in the Baltic shield, *Nature,* **348,** 34–38.

BABEL Working Group, 1993a. Integrated seismic studies of the Baltic shield using data in the Gulf of Bothnia region, *Geophys. J. Int.,* **112,** 305–324.

BABEL Working Group, 1993b. Deep seismic reflection/refraction interpretation of the crustal structure along BABEL profiles A and B in the southern Baltic Sea, *Geophys. J. Int.,* **112,** 325–343.

Birch, F., 1961. The velocity of compressional waves in rocks to 10 kilobars (Part II), *J. geoph. Res.,* **65,** 1083–1102.

Bock, G. & SVEKALAPKO Seismic Tomography Working Group, 2001. Seismic probing of Fennoscandian lithosphere, *EOS, Trans. Am. geophys. Un.,* **82**(621), 628–629.

Bogdanova, S. *et al.*, 2006. EUROBRIDGE: new insight into the geodynamic evolution of the East European Craton, in *European Lithosphere Dynamics,* pp. 599–625, eds Gee, D. & Stephenson, R. Geological Society Memoir 32, The Geological Society, London.

Bruneton, M., Farra, V., Pedersen, H. & the SVEKALAPKO STWG, 2002. Non-linear surface wave phase velocity inversion based on ray theory, *Geophys. J. Int.,* **151**(2), 583–596.

Bruneton, M. *et al.*, 2004a. Layered lithospheric mantle in the central Baltic Shield from surface waves and xenoliths analysis, *Earth planet. Sci. Lett.,* **226,** 41–52.

Bruneton, M. *et al.*, 2004b. Complex lithospheric structure under the central Baltic Shield from surface wave tomography. *J. geophys. Res.-Solid Earth,* **109**(B10), art. no. B10303.

Chevrot, S., Vinnik, L.P. & Montagner, J.P., 1999. Global-scale analysis of the mantle Pds phases, *J. geophys. Res.,* **101,** 20 203–20 219.

Christensen, N.I. & Mooney, W.D., 1995. Seismic velocity and composition of the continental crust: a global view, *J. geoph. Res.,* **100,** 9761–9788.

Darbyshire, F.A., Eaton, D.W., Frederiksen, A.W. & Ertolahti, L., 2007. New insights into the lithosphere beneath the Superior Province from Rayleigh wave dispersion and receiver function analysis, *Geoph. J. Int.,* **169,** 1043–1068.

Dricker, I.G., Kosarev, G.L., Roecker, L.P. & Vinnik, L.P., 1996. Shear-wave velocity structure of the crust and upper mantle beneath the Kola peninsula, *Geoph. Res. Lett.,* **23**(23), 3389–3392.

Eaton, D.W., 2006. Multi-genetic origin of the continental Moho: insights from LITHOPROBE, *Terra Nova,* **18**(1), 34–43.

Eaton, D.W., Dineva, S. & Mereu, R., 2006. Crustal thickness and Vp/Vs variations in the Grenville orgen (Ontario, Canada) from analysis of teleseismic receiver functions, *Tectonophysics,* **420**(1–2), 223–238.

FENNIA Working Group, 1998. P- and S-velocity structure of the Baltic Shield beneath the FENNIA profile in southern Finland, Report S-38, Institute of Seismology, University of Helsinki, Helsinki.

Gorbatschev, R. & Bogdanova, S., 1993. Frontiers in the Baltic Shield, *Precambrian Res.,* **64,** 3–21.

Grad, M. & Luosto, U., 1987. Seismic models of the crust of the Baltic Shield along the SVEKA profile in Finland, *Ann. Geophys.,* **5B,** 639–650.

Grad, M. & Luosto, U., 1994. Seismic velocities and Q-factors in the uppermost crust beneath the SVEKA profile in Finland, *Tectonophysics,* **230,** 1–18.

Griffin, W.L., O'Reilly, S.Y., Abe, N., Aulbach, S., Davies, R.M., Pearson, N.J., Doyle, B.J. & Kivi, K., 2003. The origin and evolution of Archaean lithospheric mantle, *Precambrian Res.,* **127,** 19–41.

Haskell, N.A., 1962. Crustal reflection of plane P and SV waves, *J. geophys. Res.,* **67,** 4751–4767.

Heikkinen, P. & Luosto, U., 2000. Review of some features of the seismic velocity models in Finland, in *Proceedings of LITHOSPHERE 2000. A Symposium on the Structure, Composition and Evolution of the Lithosphere in Finland* (Extended Abstracts), pp. 35–41, eds Pesonen, L., Korja, A. & Hjelt, S.-E., GSF, Espoo, 4–5.10.2000.

Henkel, H., Lee, M.K. & Lund, C.-E., 1990. An integrated geophysical interpretation of the 2000 km FENNOLORA section of the Baltic Schield, in *The European Geotraverse: Integrative Studies,* pp. 1–48, eds Freeman, R., Giese, P. & Mueller, St., ESF.

Hjelt, S.-E., Daly, S. & SVEKALAPKO Colleagues, 1996. SVEKALAPKO Evolution of Paleoproterozoic and Archaean Lithosphere, in *EUROPROBE-1996 Lithosphere Dynamics: Origin and Evolution of Continents,* pp. 57–67, Gee, D.G.& Zeyen, H.J, EUROPROBE Secretariat, Uppsala University.

Hjelt, S-E., Korja, T., Kozlovskaya, E., Yliniemi, J., Lahti, I. & BEAR and SVEKALAPKO Working Groups, 2006. Electrical conductivity and seismic velocity structures of the lithosphere beneath the Fennoscandian Shield, in *European Lithosphere Dynamics,* pp. 541–559, eds Gee, D. & Stephenson, R. Geological Society Memoir 32, The Geological Society, London.

Hyvönen, T., Tiira, T., Korja, A., Heikkinen, P., Rautioaho, E. & SVEKALAPKO Seismic Tomography Working Group, 2007. A tomographic crustal velocity model of the central Fennoscandia Shield, *Geophys. J. Int.,* **168,** 1210–1226.

Ingber, L., 1989. Very fast simulated re-annealing, *Math. Comput. Model.,* **12,** 967–973.

Isaacs, E.H. & Srivastava, R.M., 1989. *Applied Geostatistics,* Oxford Univ. Press, New York, 80 pp.

Janik, T., Kozlovskaya, E. & Yliniemi, J., 2007. Crust-mantle boundary in the central Fennoscandian shield: constraints from wide-angle P- and S-wave velocity models and new results of reflection profiling in Finland, *J. geophys. Res.,* **112,** B04302, doi:10.1029/2006JB004681.

Julia, J., Ammon, C.J., Herrmann, R.B. & Correig, A. M., 2000. Joint inversion of receiver function and surface-wave dispersion observations, *Geophys. J. Int.,* **143,** 191–202.

Kind, R., Kosarev, G.L., Petersen, N.V., 1995. Receiver functions at the stations of the German Regional Seismic Network (GRSN), *Geophys. J. Int.,* **21,** 191–202.

Kobussen, A.F., Christensen, N.I. & Thubo, H., 2006. Constraints on seismic velocity anomalies beneath the Siberian craton from xenoliths and petrophysics, *Tectonophysics,* **425,** 123–135.

Komminaho, K. & Yliniemi, J., 1993. Combined interpretation of P- and S-wave data along the BABEL lines 3 and 4 in the northern part of the Gulf of Bothnia, in *The BABEL Project,* First Status Report, Comission of the European Communities, eds Meissner, R., Snyder, D., Balling, N. & Staroste, E., Directorate-General XII. Science (Research and Development), Brussels.

Korja, A., Korja, T., Luosto, U. & Heikkinen, P., 1993. Seismic and geoelectric evidence for collisional and extensional events in the Fennoscandian Schield- implications for Precambrian crustal evolution, *Tectonophysics,* **219,** 129–152.

Korja, A., Lahtinen, R., Heikkinen, P., Kukkonen, I.T. & FIRE Working Group, 2006. A geological interpretation of the upper crust along FIRE1, *Geological Survey of Finland* (Special paper), **43,** 45–76.

Korsman, K., & Koistinen, T., 1998. Suomen Kalioperän ylieispiirteet, in *3000 Vuosi-miljoonaa, Suomen Kallioperä (Bedrock of Finland)*, pp. 93–103, eds Lehtinen, M., Nurmi, P., Rämö, T., Suomen Geologinen Seura (Finnish Geological Society) (in Finnish).

Korsman, K., Korja, T., Pajunen, M., Virransalo, P. & the GGT/SVEKA Working Group, 1999. The GGT/SVEKA transect: structure and evolution of the continental crust in the Paleoproterozoic Svecofennian Orogen in Finland, *Int. Geol. Rev.,* **41,** 287–333.

Kozlovskaya, E. & Yliniemi, J., 1999. Deep structure of the Earth's crust along the SVEKA profile and its extention to the north-east, *Geophysica,* **1-2,** 111–123.

Kozlovskaya, E., Elo, S., Hjelt, S.-E., Yliniemi, J., Pirttijärvi, M. & SVEKALAPKO Seismic Tomography Working Group, 2004a. 3D density model of the crust of southern and central Finland obtained from joint interpretation of SVEKALAPKO crustal P-wave velocity model and gravity data, *Geophys. J. Int.,* **158,** 827–848.

Kozlovskaya, E., Janik, T., Yliniemi, J., Karatayev, G. & Grad, M., 2004b. Density-velocity relationship in the upper lithosphere obtained from P- and S-wave velocity models along the EUROBRIDGE'97 wide-angle reflection and refraction profile and gravity data, *Acta Geophysica Polonia,* **52**(4), 397–424.

Krasovsky, S.S., 1981. *Reflection of Continental-type Crustal Dynamics in the Gravity Field* (in Russian), Navukova Dumka, Kiev.

Kukkonen, I.T., Kinnunen, K.A. & Peltonen, P., 2003. Mantle xenoliths and thick lithosphere in the Fennoscandian Shield, *Phys. Chem. Earth,* **28,** 349–360.

Kukkonen, I.T., Heikkinen, P., Ekdahl, E., Hjelt, S.-E., Yliniemi, J., Jalkanen, E. & FIRE Working Group, 2006. Aquisition and geophysical characteristics of reflection seismic data on FIRE transects, Fennoscandian Shield, *Geological Survey of Finland* (Special paper), **43,** 13–43.

Lahtinen, R., Korja, A. & Nironen, M., 2005. Palaeoproterozoic tectonic evolution of the Fennoscandian Shield – a plate tectonic model, in *The Precambrian Bedrock of Finland – Key to the Evolution of the Fennoscandian Shield,* Precambrian Series, eds Lehtinen, M., Nurmi, P. & Rämö, T., Elsevier Science B.V., Amsterdam.

Lombardi, D., Braunmiller, J., Kissling, E. & Giardini, D., 2006. Moho depth and Poisson's ratio in the Western-central Alps from receiver functions, *Geophys. J. Int.,* **173**(1), 249–264.

Luosto, U., 1991. Moho depth map of the Fennoscandian Shield based on seismic refraction data, in *Structure and Dynamics of the Fennoscandian Lithosphere,* Report S-25, pp. 43–49, eds Korhonen, H. & Lipponen, A., Institute of Seismology, University of Helsinki.

Luosto, U., 1997. Structure of the Earth's crust in Fennoscandia as revealed from refraction and wide-angle reflection studies, *Geophysica,* **33,** 3–16.

Luosto, U., Lanne, E., Korhonen, H., Guterch, A., Grad, M., Materzok, R. & Perchuć, E., 1984. Deep structure of the Earth's crust on the SVEKA profile in central Finland, *Ann. Geophys.,* **2,** 559–570.

Luosto, U *et al.*, 1990. Crust and upper mantle structure along the DSS BALTIC profile in SE Finland, *Geophys. J. Int.,* **101,** 89–110.

Luosto, U. *et al.*, 1994. Crustal structure along the SVEKA'91 profile (Finland), in *Proceedings of the XXIV General Assembly of European Seismological Commission,* Athens, Greece, 1994 September 19–24.

Malaska, J. & Hyvönen, T., 2000. Velocity modelling of the lithosphere beneath South Finland, *Phys. Earth planet. Inter.,* **122**(1–2), 103–114.

Musacchio, G., Mooney, W.D., Luetgert, J.H. & Christensen, N.I., 1997. Composition of the crust in the grenville and Appalachian provinces of North America inferred from Vp/Vs ratios, *J. geophys. Res,* **102,** 15 225–15 241.

Pavlenkova, N.I., Luosto, U., Yliniemi, J. & Ansorge, J., 2001. 3-D P-velocity model of the crust in the Baltic Shield, in *Proceedings of the 6th SVEKALAPKO Workshop* p. 43, ed. Hjelt, S.-E., Lammi, Finland, 2001 November 29–December 2. University of Oulu, Department of Geosciences, Report 24, Oulu.

Pearson, D.G., 1999. The age of continental roots, *Lithos,* **48,** 171–194.

Pedersen, H. & Campillo, M., 1991. Depth dependence of Q beneath the Baltic Shield inferred from modelling of short period seismograms, *Geophys. Res. Lett.,* **18**(9), doi:10.1029/91GL01693.

Pedersen, H., Bruneton, M., Maupin, V. & SVEKALAPKO Seismic Tomography Working Group, 2006. Lithospheric and sublithospheric anisotropy beneath the Baltic Shield from surface-wave array analysis, *Earth planet. Sci. Lett.,* **244,** 590–605.

Pedersen, H. Krüger, F. & the SVEKALAPKO Seismic Tomography Working Group, 2007. Influence of the seismic noise characteristics on noise correlations in the Fennoscandian Shield, *Geophys. J. Int.,* **168,** 197–210.

Peltonen, P., Mänttäri, I., Huhma, H. & Whitehouse, M., 2006. Multi-stage origin of the lower crust of the Karelian craton from 3.5 to 1.7 Ga based on isotopic ages of kimberlite-derived mafic granulite xenoliths, *Precambrian Res.,* **147,** 107–123.

Plomerova, J., Babuska, V., Vecsey, L., Kozlovskaya, E., Raita, T. & SVEKALAPKO STWG, 2006. Proterozoic-Archean boundary in the upper mantle of eastern Fennoscandia as seen by seismic anisotropy, *J. Geodyn.,* **41**(4), 369–450.

Proskuryakova, T.A, Novotny, O. & Voronina, E.V., 1981. *Studies of the Earth's Structure by Surface Waves Method (Central Europe),* p. 94, Nauka, Moscow.

Sandoval, S., 2002. The lithosphere-asthenosphere system beneath Fennoscandia (Baltic Shield) by body-wave tomography, *PhD thesis*. ETH, Zürich.

Sandoval, S., Kissling, E., Ansorge, J. & the SSTWG, 2003. High-resolution body wave tomo-graphy beneath the SVEKALAPKO array, I: a priori 3D crustal model and associated travel time effcets on teleseismic wave fronts, *Geophys. J. Int.,* **153,** 75–87.

Sandoval, S., Kissling, E., Ansorge, J. & SVEKALAPKO STWG, 2004. High-resolution body wave tomography beneath the SVEKALAPKO array, II: anomalous upper mantle structure beneath the central Baltic Shield, *Geophys. J. Int.,* **157,** 200–214.

Sharov, N.V., 1991. Lithosphere of the Baltic schield according to seismic data, in *Structure and dynamics of the Fennoscandian lithosphere,* Report S-25, pp. 1–6, Institute of seismology, University of Helsinki.

Silvennoinen, H. & Kozlovskaya, E., 2007. 3-D structure and physical properties of the Kuhmo Greenstone Belt (eastern Finland): constraints from gravity modelling and petrophysical data, *J. Geodyn.,* **43**(3), 358–373.

Sobolev, S.V. & Babeyko, A.Y., 1994. Modeling of mineralogical composition, density and elastic wave velocities in anhydrous magmatic rocks, *Surv. geophys.,* **15,** 515–544.

Tarantola, A., 1987. *Inverse Problem Theory, Elsevier Science*, New York.

Vecsey, L., Plomerova, J., Kozlovskaya, E. & Babuska, V., 2007. Shear-wave splitting as a diagnostic of varying upper mantle structure beneath eastern Fennoscandia, *Tectonophysics,* **438**(1–4), 57–77.

Vinnik, L.P., 1977. Detection of waves converted from P to SV in the mantle, *Phys. Earth planet. Inter.,* **15,** p . 39–45

Vinnik, L.P., Reigber, C., Aleshin, I.M., Kosarev, G.L., Kaban, M.K., Oreshin, S.I. & Roecker, S.W., 2004. Receiver function tomography of the central Tien Shan, *Earth Phys. Sci. Lett.,* **225,** 131.

Vinnik, L.P., Aleshin, I.M., Kaban, M.K., Kiselev, S.G., Kosarev, G.L., Oreshin, S.I. & Reigber, Ch., 2006. Crust and mantle of the Tien Shan from data of the receiver function tomography, *Phys. Solid Earth,* **42**(8), 639–651.

Yliniemi, J., 1991. Deep seismic soundings in the University of Oulu, in *Structure and Dynamics of the Fennoscandian Lithosphere,* Report S-25, pp. 1–6, Institute of seismology, University of Helsinki.

Yliniemi, J., Kozlovskaya, E., Hjelt, S-E., Komminaho, K., Ushakov, A. & the SVEKALAPKO Tomography WG, 2004. Structure of the crust and uppermost mantle beneath southern Finland revealed by local events registered by the SVEKALAPKO seismic array, *Tectonophysics,* **394,** 41–67.

Zhu, L. & Kanamori, H., 2000. Moho depth variations in southern California from teleseismic receiver functions, *J. geophys. Res.,* **105,** 2969–2980.